IV International Conference on Particle Physics and Astrophysics
October 22-26, 2018

STAR Highlights and Future

Grigory Nigmatkulov
(for the STAR Collaboration)
National Research Nuclear University
MEPhI

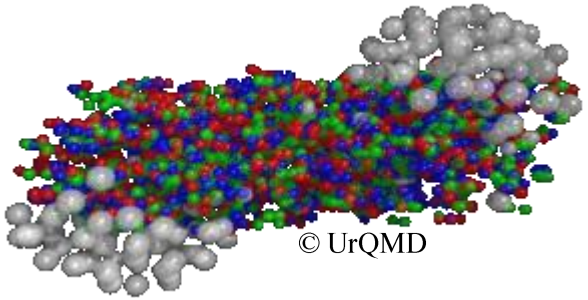

Outline:

- Introduction
- Collective Dynamics and Correlations
- Global Polarization
- Particle Production
- High-p_T Hadrons and Jet Modification
- The STAR Fixed-Target Program
- Detector Upgrades

Introduction

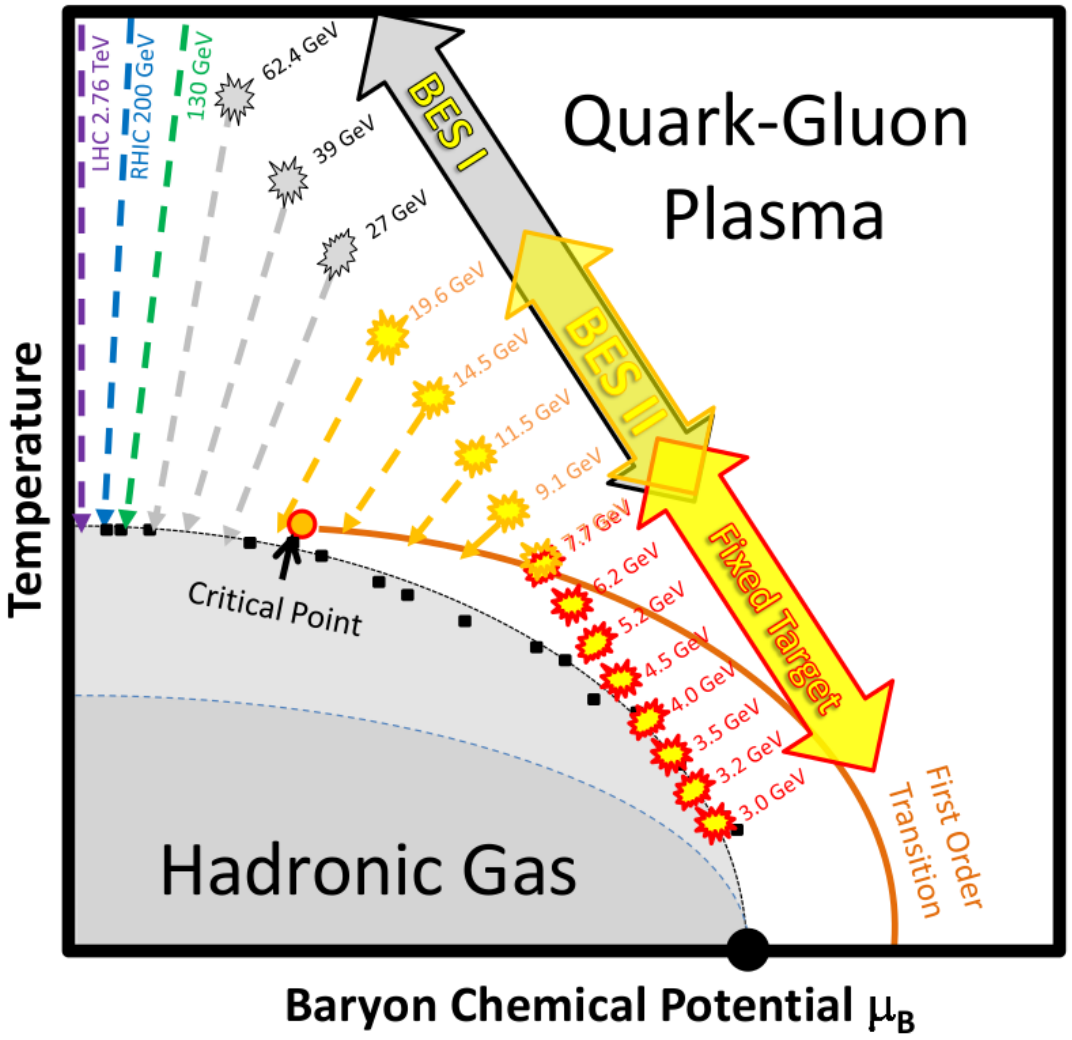

Top RHIC energy

p+p, p+Al, p+Au, d+Au, ^{3}He+Au, Cu+Cu, Cu+Au, Ru+Ru, Zr+Zr, Au+Au, U+U

- QCD at high energy density/temperature
- Properties of QGP, Equation of State (EoS)
- Proton spin structure

Beam Energy Scan

Au+Au $\sqrt{s_{NN}}$=7.7-62.4 GeV

- Search for critical point
- QCD phase transition
- Turn-off of QGP signatures

Fixed-Target Program

Au+Au $\sqrt{s_{NN}}$=3.0-7.7 GeV

- High baryon density (μ_B~420-720 MeV)

The STAR ☆ Experiment

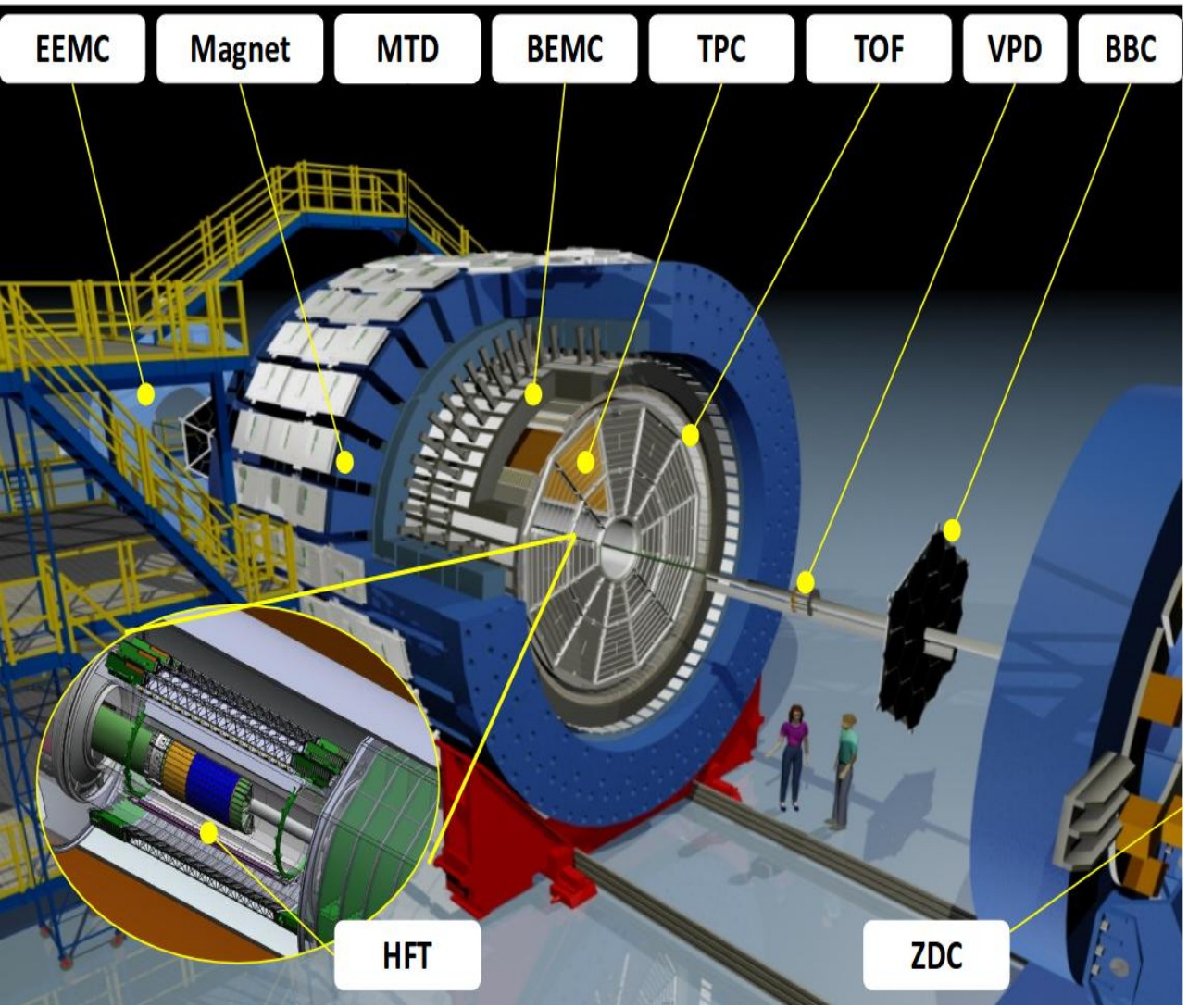

- **Tracking and PID (full 2π)**
  TPC: |η|<1
  TOF: |η|<1
  BEMC: |η|<1
  EEMC: 1<|η|<2
  HFT (2014-2016): |η|<1
  MTD (2014+): |η|<0.5

- **MB trigger and event plane reconstruction**
  BBC: 3.3<|η|<5
  EPD (2018+): 3.1<|η|<5.1
  FMS: 2.5<|η|<4
  VPD: 4.2<|η|<5
  ZDC: 6.5<|η|<7.5

- **On-going/future upgrades**
  iTPC (2019+): |η|<1.5
  eTOF (2019+): -1.6<η<-1
  FCS (2021+): 2.5<η<4
  FTS (2021+): 2.5<η<4

Particle Identification with TPC and TOF

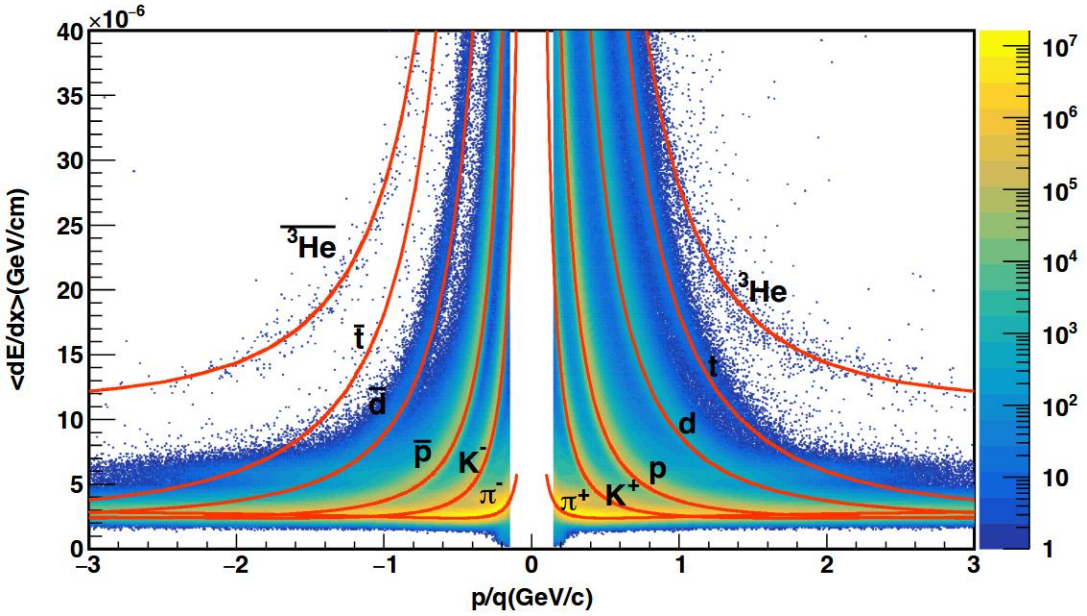

- The <dE/dx> versus rigidity measured by TPC in 2014 Au+Au collisions at $\sqrt{s_{NN}}$=200 GeV

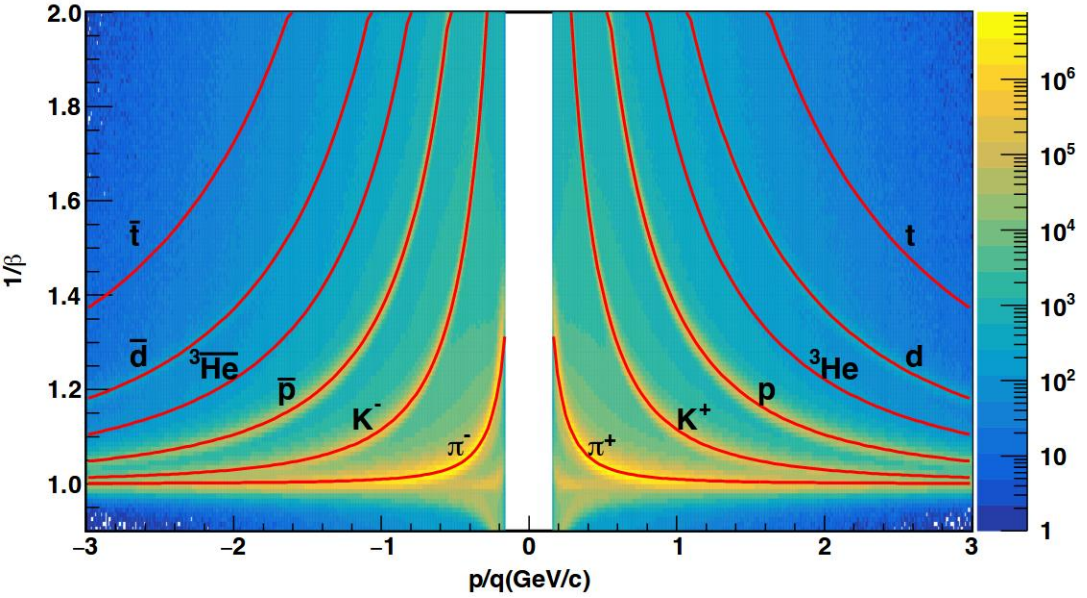

- The 1/β versus rigidity measured by TOF in 2014 Au+Au collisions at $\sqrt{s_{NN}}$=200 GeV

Azimuthal Anisotropy in Heavy-Ion Collisions

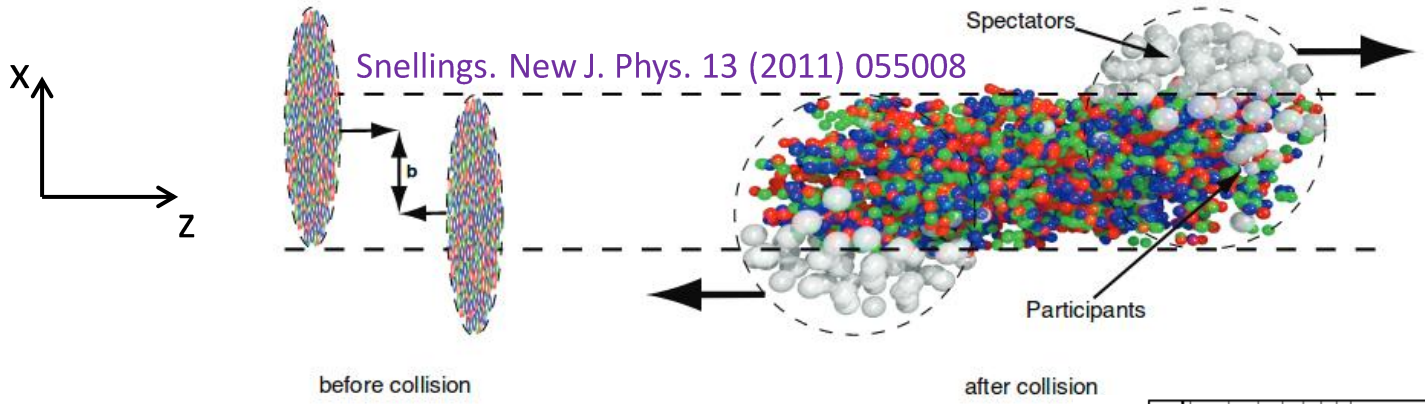

Snellings. New J. Phys. 13 (2011) 055008

$$E\frac{d^3N}{d^3p} = \frac{1}{2\pi}\frac{d^2N}{p_t dp_t dy}\left(1+\sum_{n=1}^{\infty} 2v_n\cos[n(\phi-\Psi_r)]\right)$$

Voloshin , Zhang. Z. Phys. C 70 (1996) 665
Poskanzer, Voloshin. Phys. Rev. C 58 (1998) 1671

- $v_1=\langle p_x/p_t\rangle$ – directed flow
- Describes the sideward collective motion of particles within the reaction plane (x-z)
- Probe of the softening of the EoS:
  - Strong softening: consistent with the 1st-order phase transition
  - Weaker softening: more likely due to crossover

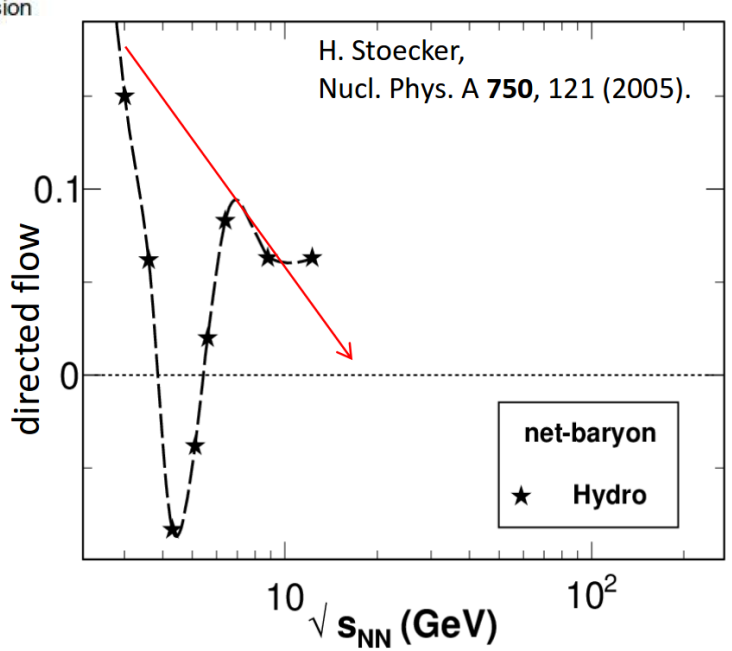

Nara, Niemi, Steinheimer, Stöker. Phys. Lett. B 769 (2017) 543
Ivanov, Soldatov. Phys. Rev. C 91 (2015) 024915

Beam-energy Dependence of Directed Flow

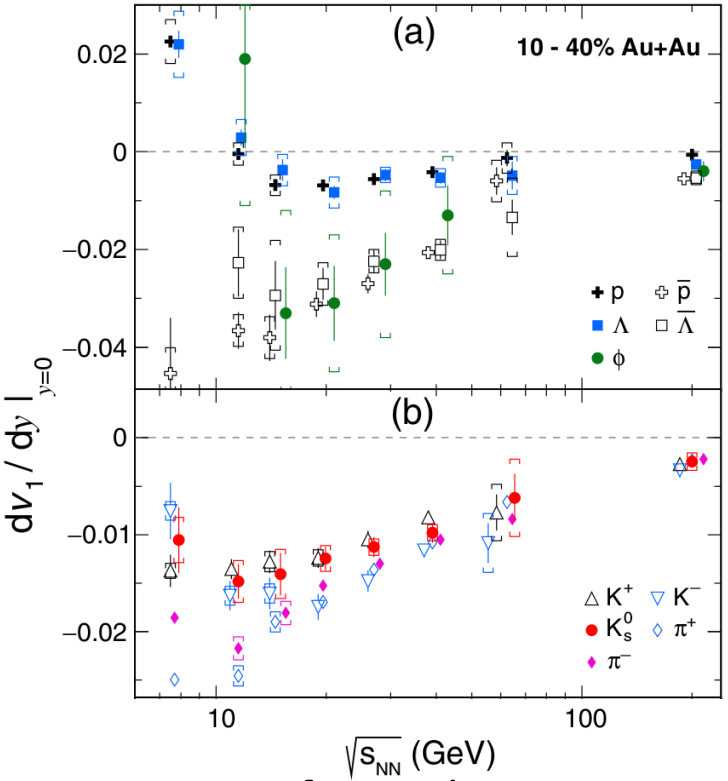

- dv_1/dy for Λ and p agree within uncertainties
- dv_1/dy slope for baryons changes sign in the region $\sqrt{s_{NN}}$<14.5 GeV
- Particles (anti-p, anti-Λ, and ϕ) with produced quarks show similar behavior for $\sqrt{s_{NN}}$>14.5 GeV
- Mesons show negative dv_1/dy

STAR. Phys. Rev. Lett. 120 (2018) 062301

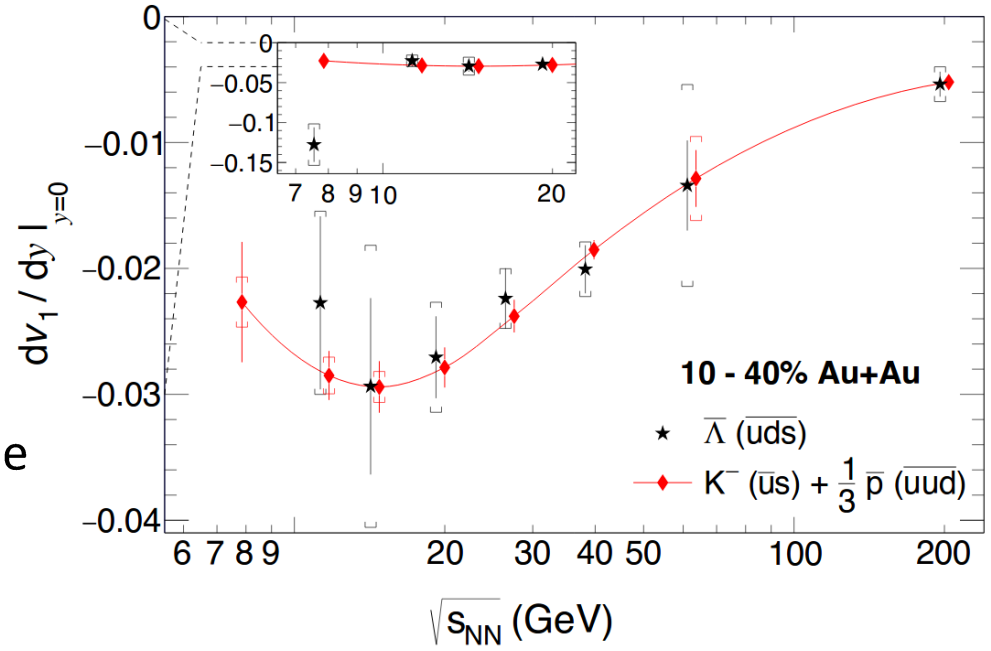

Assumptions for coalescence sum rule:

- v_1 is developed at prehadronic stage
- Specific types of quarks have the same v_1
- Hadrons are formed via coalescence

$$(v_n)_{hadron} = \Sigma(v_n)_{\text{constituent quarks}}$$

For anti-Lambdas, prediction using coalescence sum rule agrees with measured v1 above $\sqrt{s_{NN}}$=11.5 GeV

v_1 of D^0 in Au+Au at 200 GeV

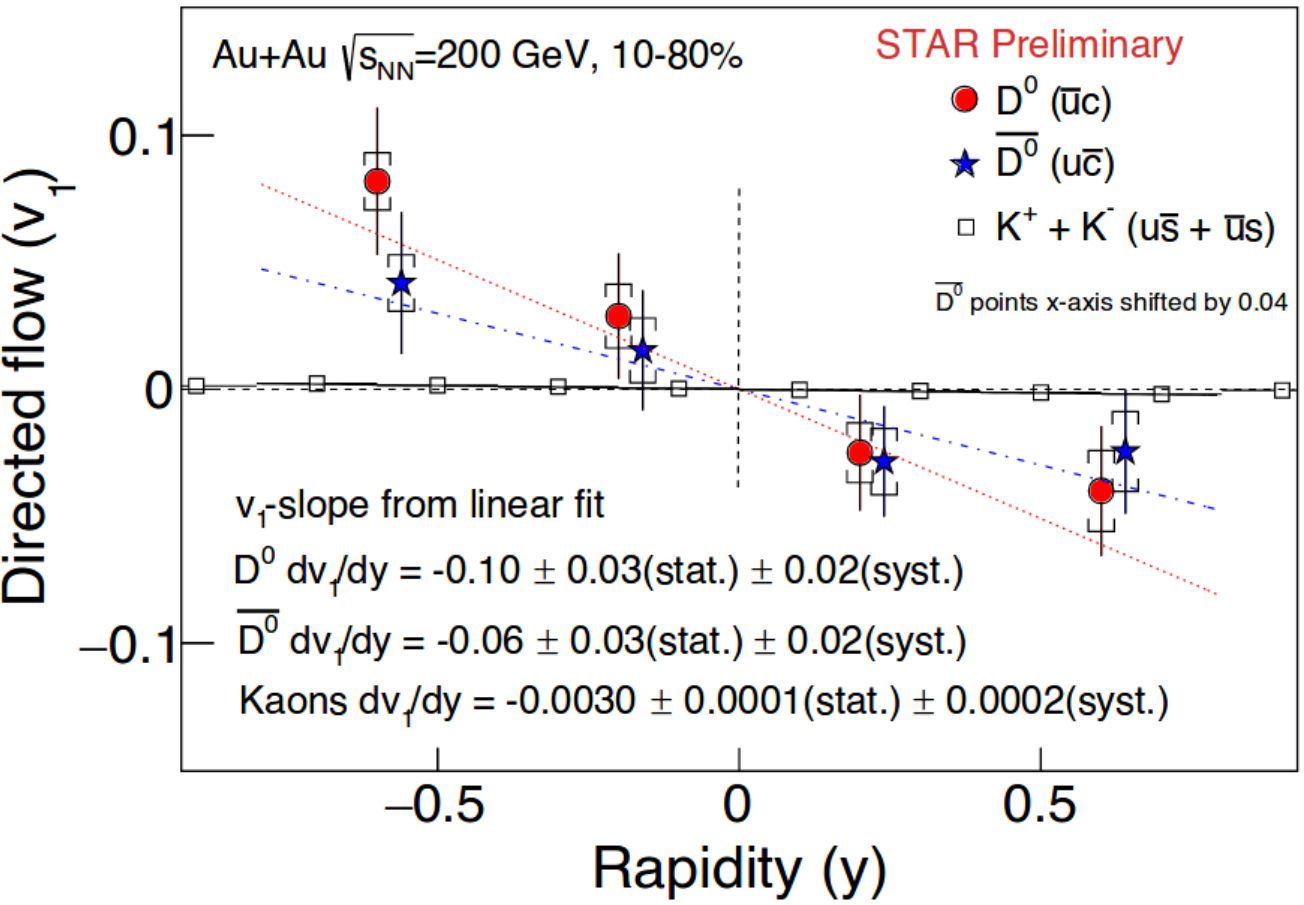

Interplay between the drag by the tilted bulk and the EM field

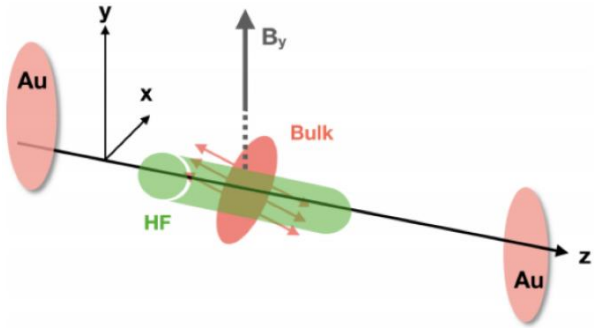

Chatterjee, Bozek. Phys. Rev. Lett. 120 (2018) 192301

First evidence for non-zero D^0 v_1 from 2014+2016 Heavy Flavor Tracker (HFT) data:

$$\boldsymbol{D^0 + \overline{D^0}\ dv_1/dy = -0.081 \pm 0.021(stat.) \pm 0.017(syst.)}$$

Longitudinal Flow Decorrelation in 200 GeV Au+Au Collisions

CMS. Phys. Rev. C 92 (2015) 034911

$$r_n(\eta) = \frac{\langle v_n(-\eta)v_n(\eta_{\rm ref})\cos n(\Psi_n(-\eta)-\Psi_n(\eta_{\rm ref}))\rangle}{\langle v_n(\ \eta)v_n(\eta_{\rm ref})\cos n(\Psi_n(\ \eta)-\Psi_n(\eta_{\rm ref}))\rangle}$$

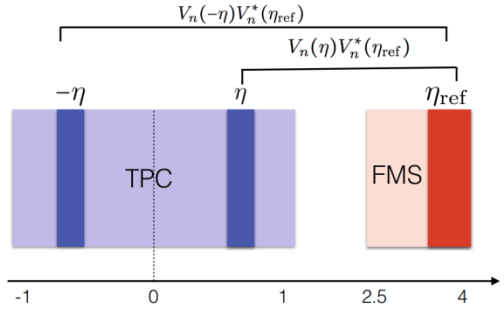

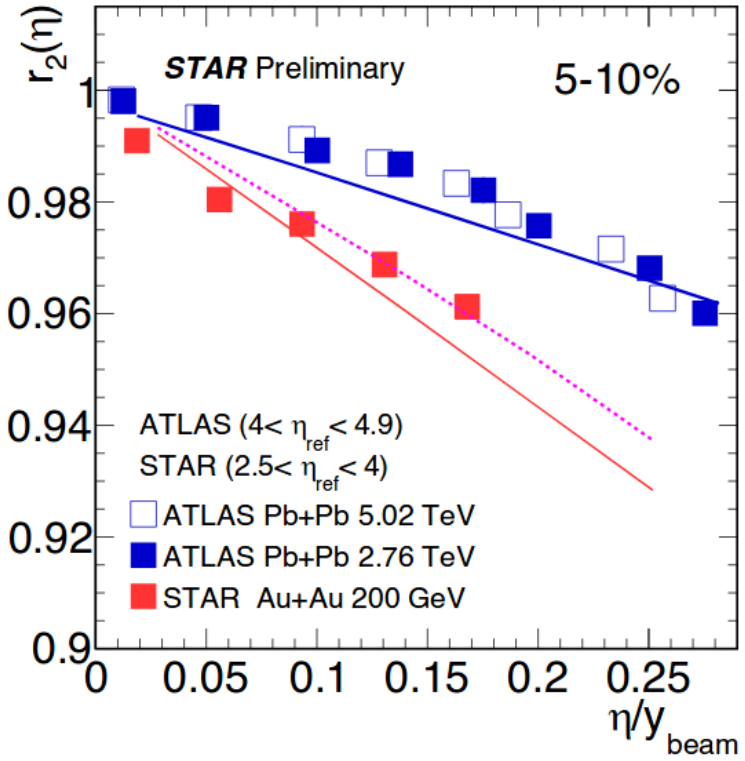

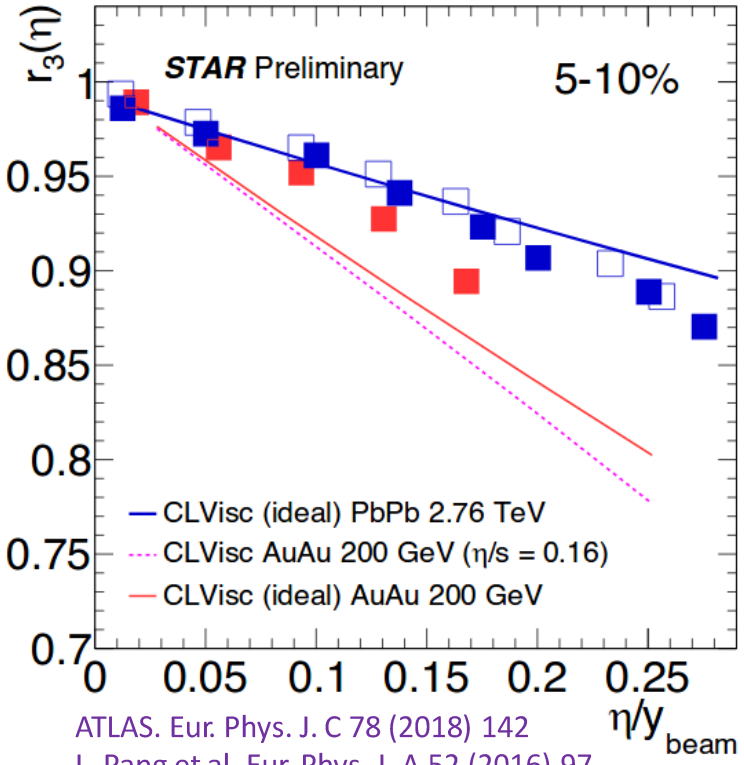

ATLAS. Eur. Phys. J. C 78 (2018) 142
L. Pang et al. Eur. Phys. J. A 52 (2016) 97
L. Pang et al. arXiv: 1802.04449

- Stronger longitudinal flow decorrelation at RHIC than at LHC
- Hydrodynamic calculations can not simultaneously describe LHC and RHIC data

Global and Local Hyperon Polarization

- New tool to study QGP and relativistic Quantum fluid Vorticity in general
- First observation of quadrupole structure of polarization along beam direction; “sign” opposite to hydro prediction

STAR. Nature 548 (2017) 62

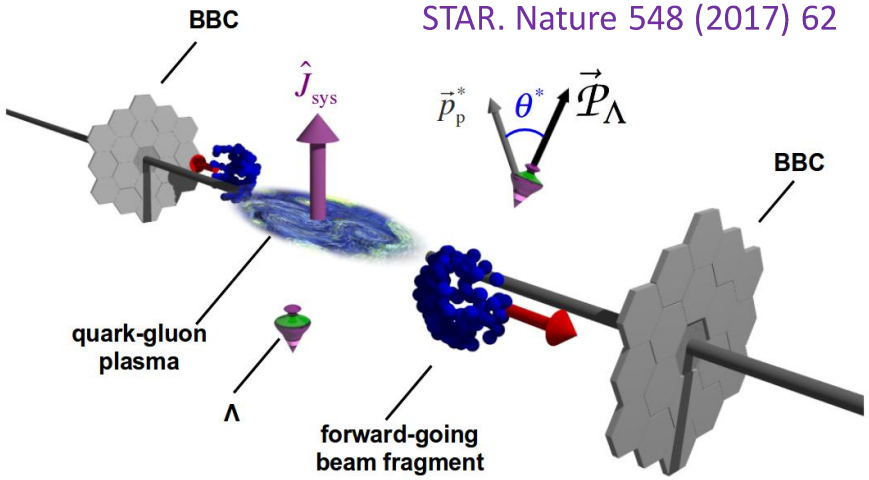

STAR. Phys. Rev. C 98 (2018) 014910

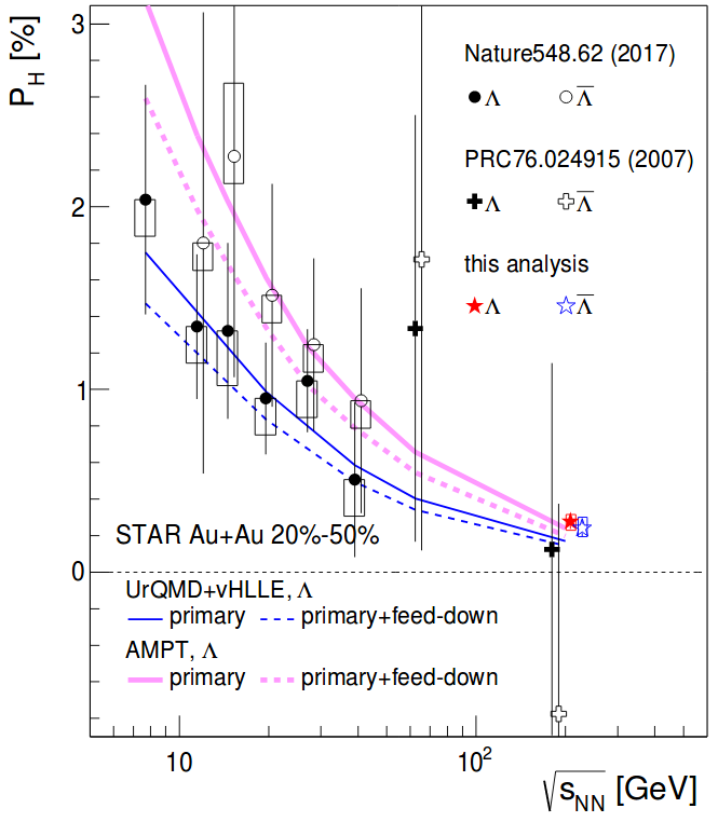

Non-zero global angular momentum transfer to hyperon polarization

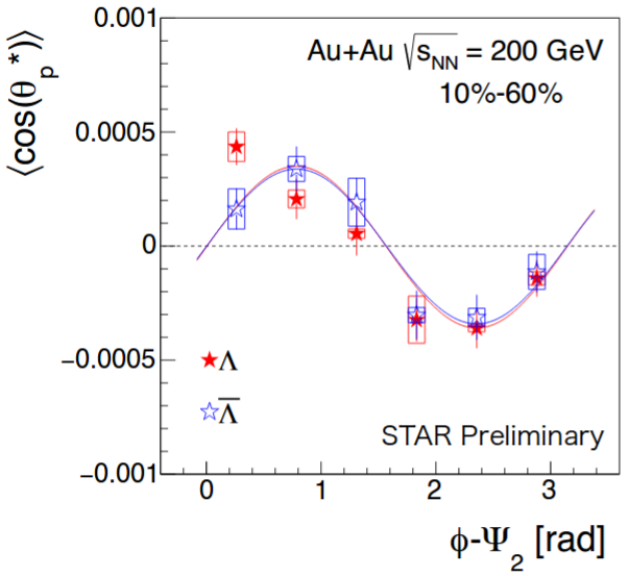

Femtoscopic Measurements

- Use two-particle momentum correlations to measure spatial and temporal properties of the source at kinetic freeze-out
- Utilizing the information from the TOF detector to extend measurement to higher transverse mass (m_T) region

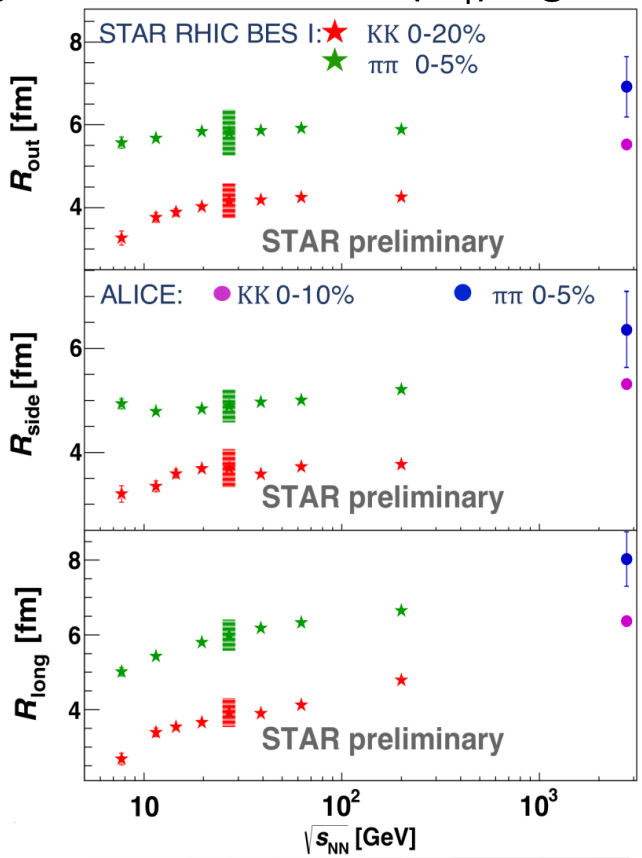

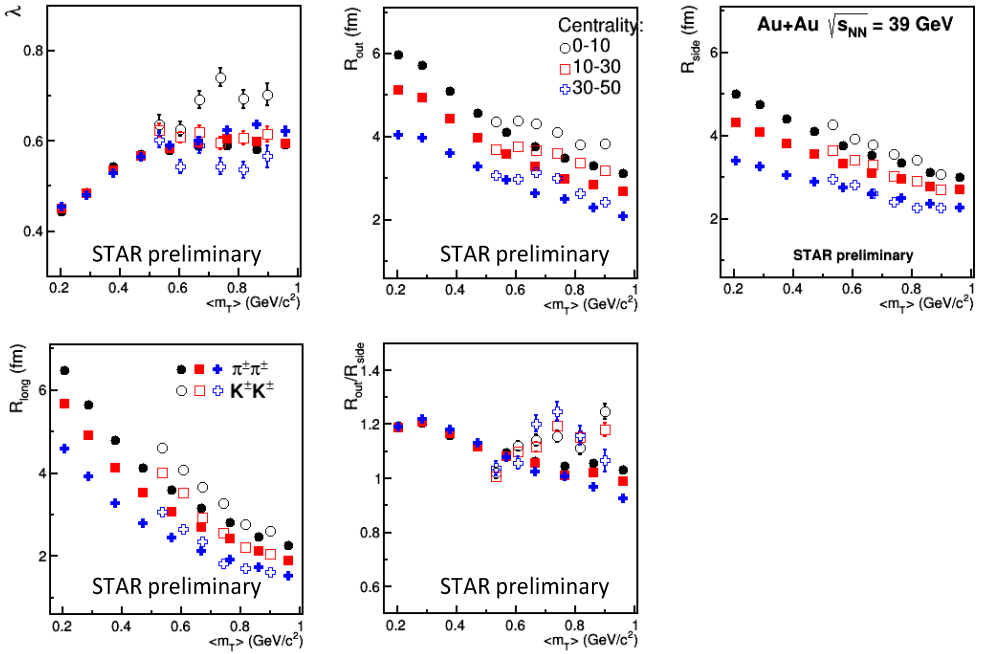

- The extracted femtoscopic radii smoothly increase with increasing collision energy
- The values of R_{out} and R_{side} for both pions and kaons show a very small increase at the RHIC energies and slightly larger at the LHC
- The values of R_{long} suggest that the system lives longer at the LHC energy

Ultra-Peripheral Collisions

Diffraction in ρ^0 photoproduction

- -t is the square of transferred 4-momentum
- Diffractive dips at –t=0.018 and 0.043 $(GeV/c)^2$
- Two cases of nuclear breakup:
  - 1n1n: one neutron at (+) and (-) rapidity
  - XnXn: one or more neutrons at (+) and (-) rapidity
- Exponential slope in dσ/dt is consistent with LHC (ALICE. JHEP 1509 (2015) 095)

Similarity in exponential parts implies no evidence for increase of nuclear size with photon energy

STAR. Phys. Rev. C 96 (2017) 054904

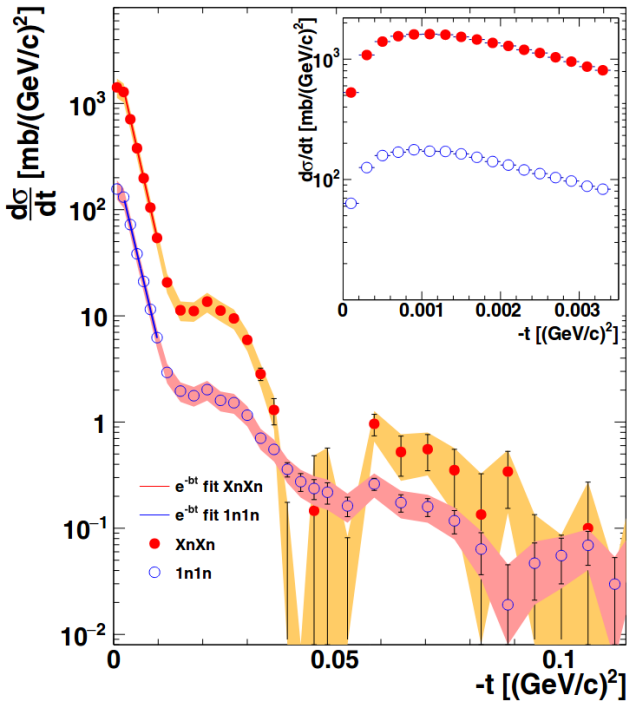

Electromagnetic processes in peripheral collisions

- Data on e^+e^- pairs in peripheral Au+Au and U+U collisions
- Yield enhanced at low p_T with respect to hadronic expectation
- Shape of the excess is consistent with e^+e^- from photoproduction

Novel probe to electromagnetic fields of the nuclei

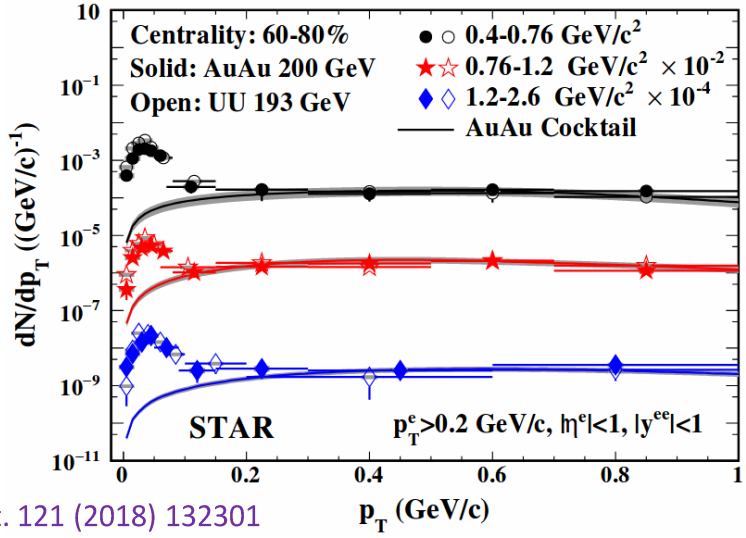

STAR. Phys. Rev. Lett. 121 (2018) 132301

(Anti)Hypertriton Binding Energy

Reconstructing ${}^{3}_{\Lambda}\mathrm{H}$ (${}^{3}_{\Lambda}\overline{\mathrm{H}}$) through:

$${}^{3}_{\Lambda}\mathrm{H} \rightarrow {}^{3}\mathrm{He} + \pi^{-}$$

$${}^{3}_{\Lambda}\mathrm{H} \rightarrow \mathrm{d} + \mathrm{p} + \pi^{-}$$

Binding energy (B_Λ) definition:

$$m_\Lambda + m_d - m_{{}^{3}_{\Lambda}\mathrm{H}}$$

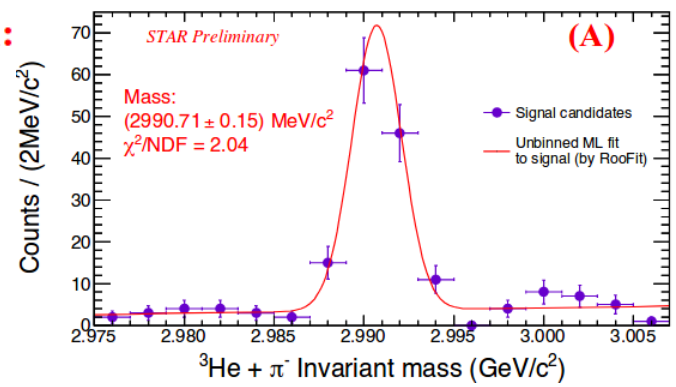

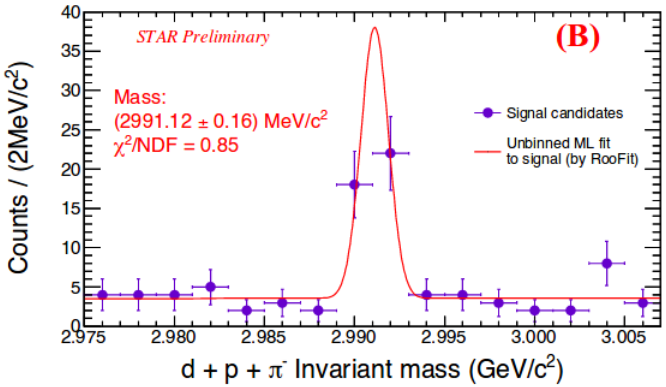

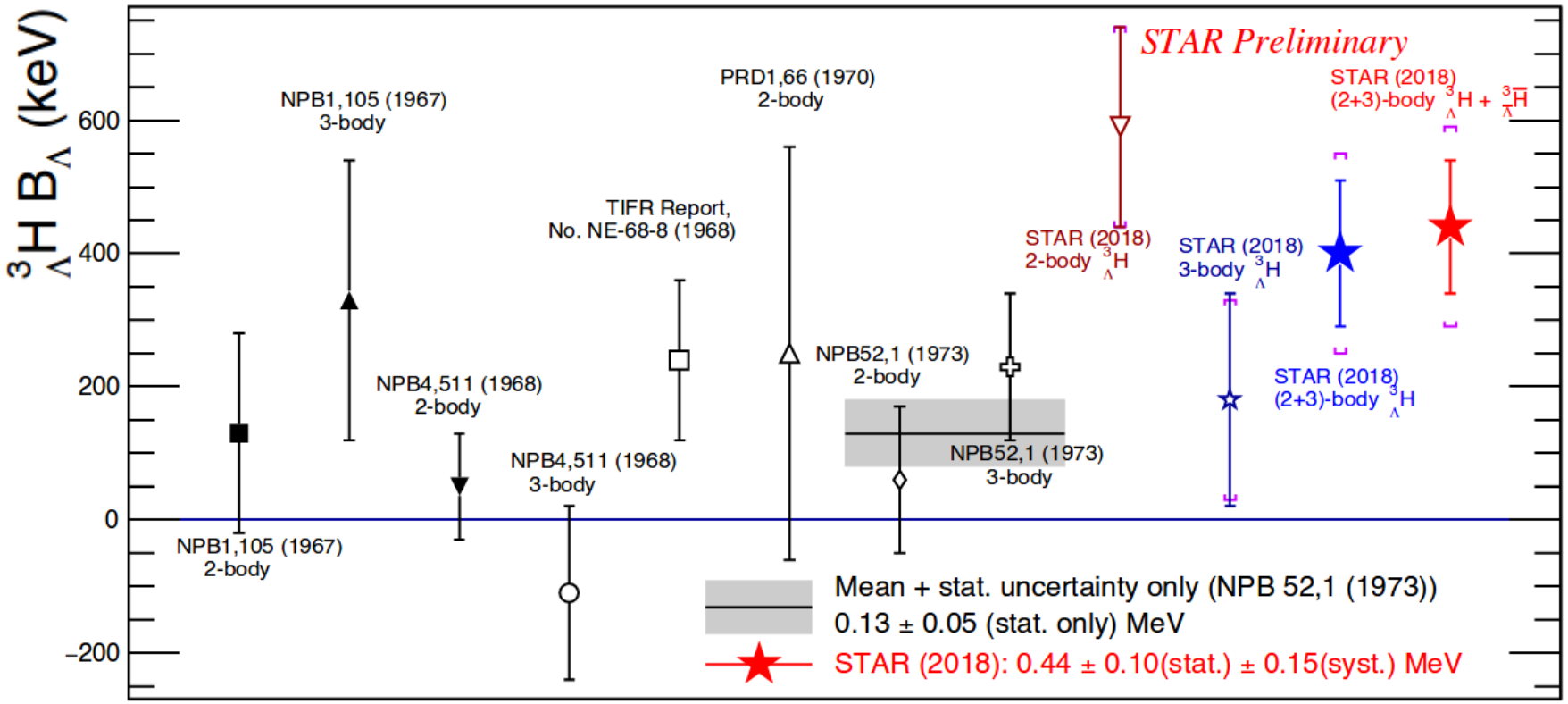

Mass Difference Between ${}^{3}_{\Lambda}H$ and ${}^{3}_{\bar{\Lambda}}\bar{H}$

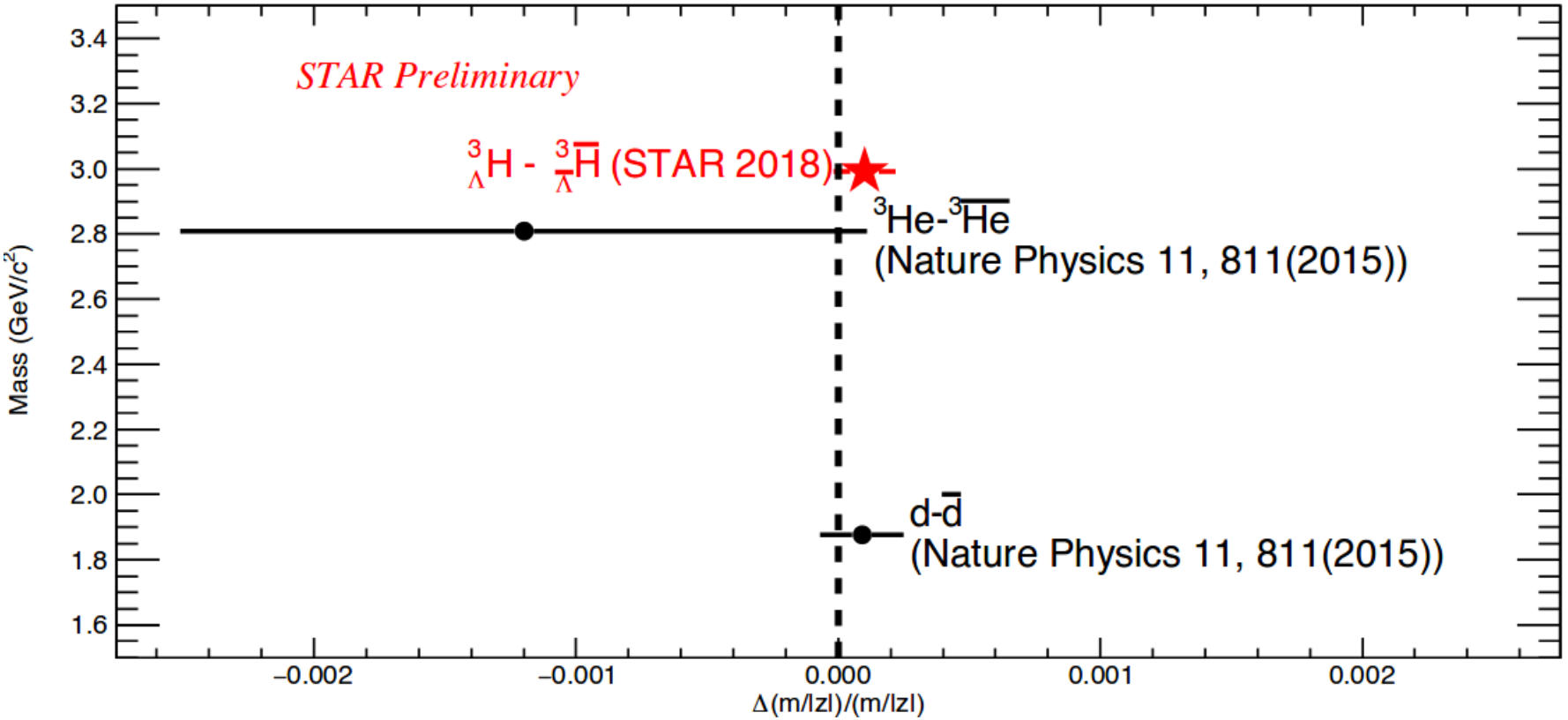

- First measurement of the hypertriton and antihypertriton mass difference
- Test of CPT symmetry in the light hypernuclei sector

$$\left(\frac{\Delta(m/|z|)}{m/|z|}\right)_{d} = (0.9 \pm 0.5\,(\text{stat.}) \pm 1.4\,(\text{syst.}))\times 10^{-4}$$

$$\left(\frac{\Delta(m/|z|)}{m/|z|}\right)_{^3\text{He}} = (-1.2 \pm 0.9\,(\text{stat.}) \pm 1.0\,(\text{syst.}))\times 10^{-3}$$

$$\left(\frac{\Delta m}{m}\right)_{^3_\Lambda\text{H}} = (1.0 \pm 0.9\,(\text{stat.}) \pm 0.7\,(\text{syst.}))\times 10^{-4}$$

- The mass difference is consistent with the CPT expectation

Λ_c Production

Adding data from year 2016 and using TMVA BDT allowed to obtain more than 2 times improvement in the signal significance than 2014 data alone

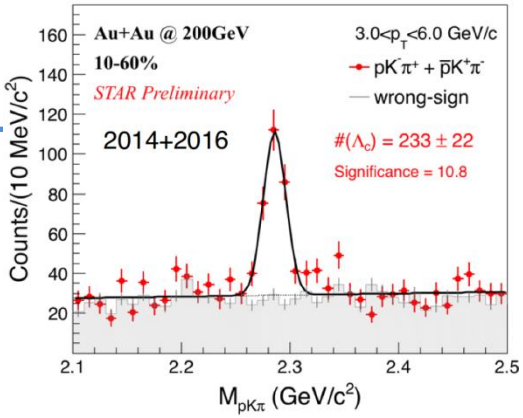

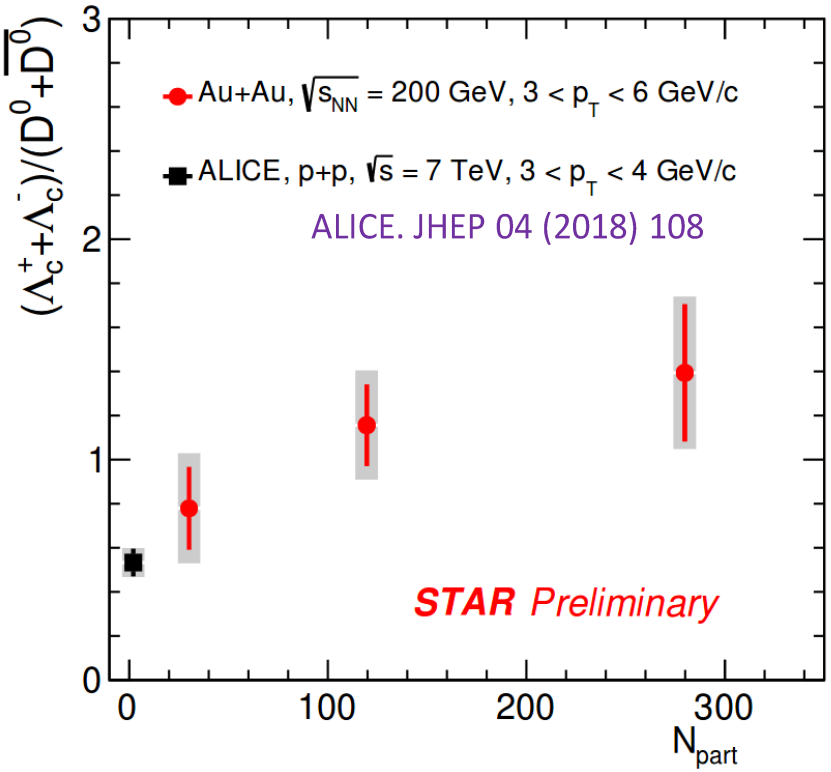

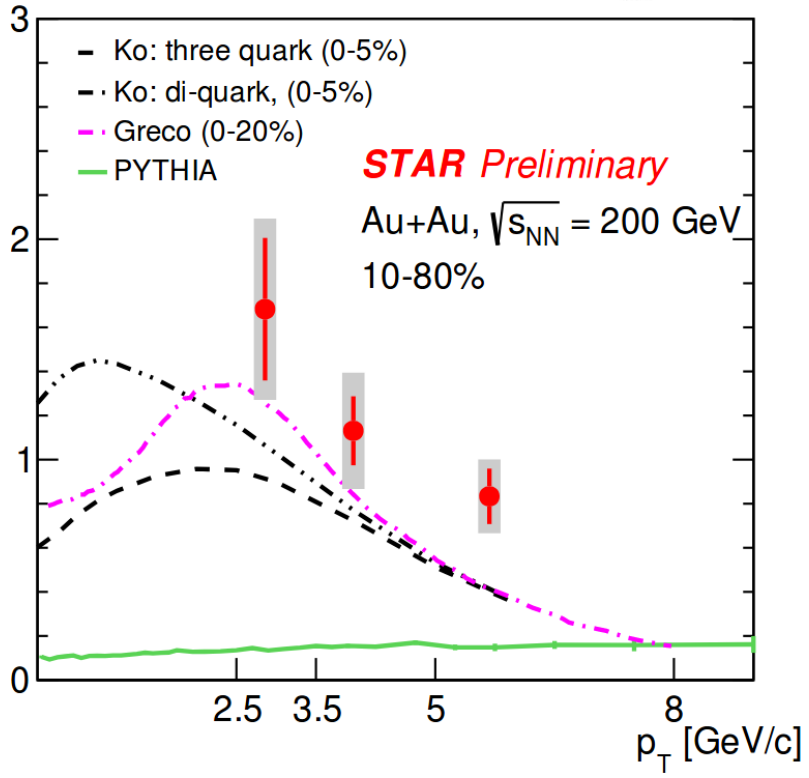

- Λ_c/D^0 ratio increases from peripheral to central collisions
- Enhancement of Λ_c production increases towards low p_T
- Large Λ_c contribution to the total charm cross-section in heavy-ion collisions

Upsilon Suppression in Au+Au @ 200 GeV

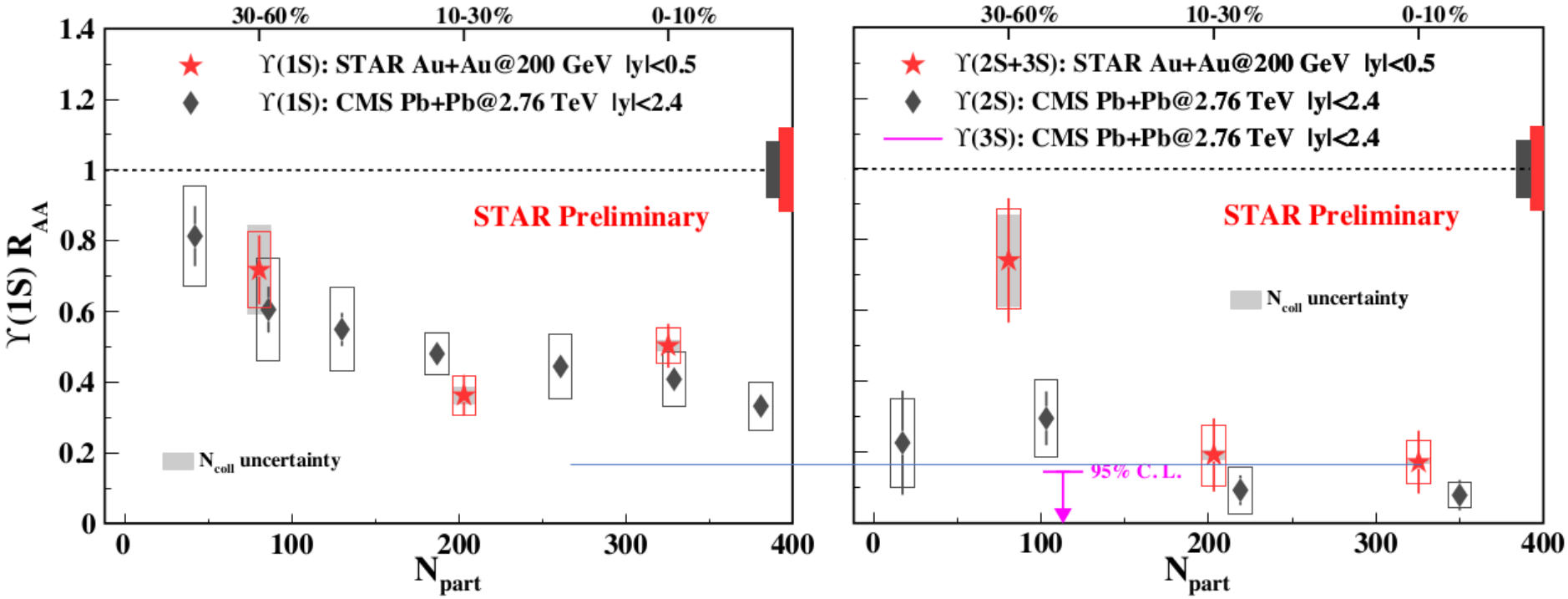

CMS. Phys. Lett. B 04 (2017) 031

- Improved precision by combining 2011 di-electron, 2014+2016 di-muon
- Υ(2S+3S) R_{AA} smaller that Υ(1S) in 0-10%
  - "Sequential melting" at RHIC

Nuclear Modification in BES-I

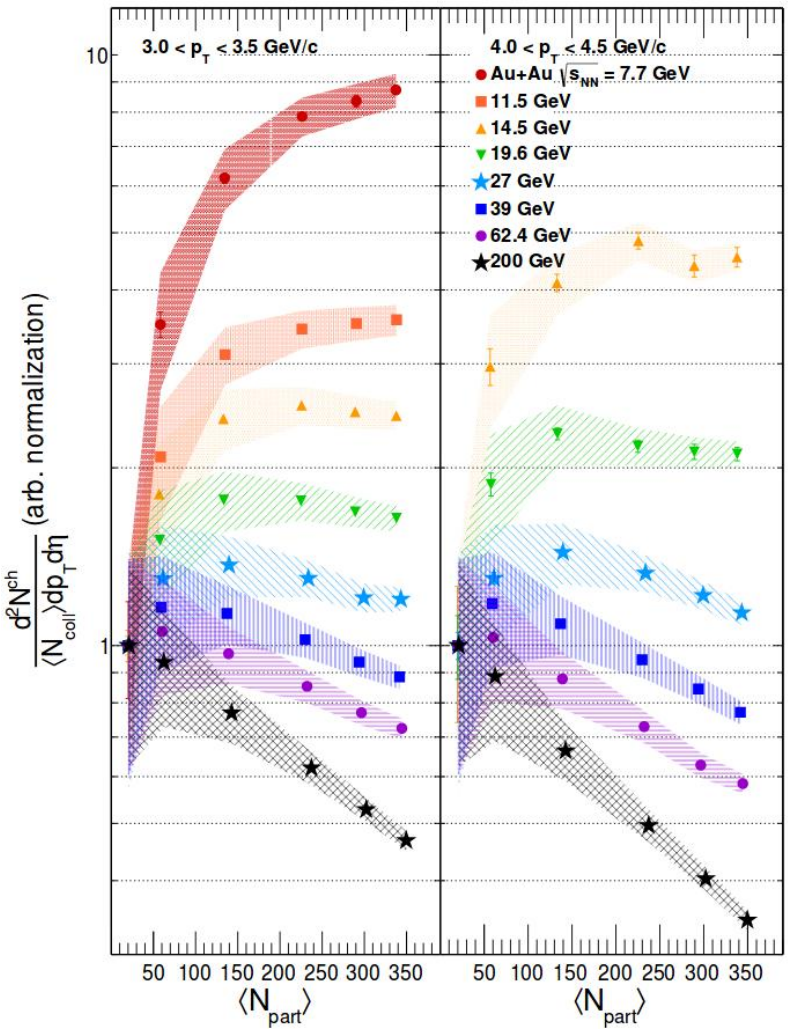

STAR. Phys. Rev. Lett. 121 (2018) 032301

- R_{CP} for hadrons and for charged particles probes partonic energy loss in the medium
- BES-I results Indicate disappearance of suppression bellow 14.5 GeV
- Would like to explore this with identified hadrons (to isolate baryon stopping)

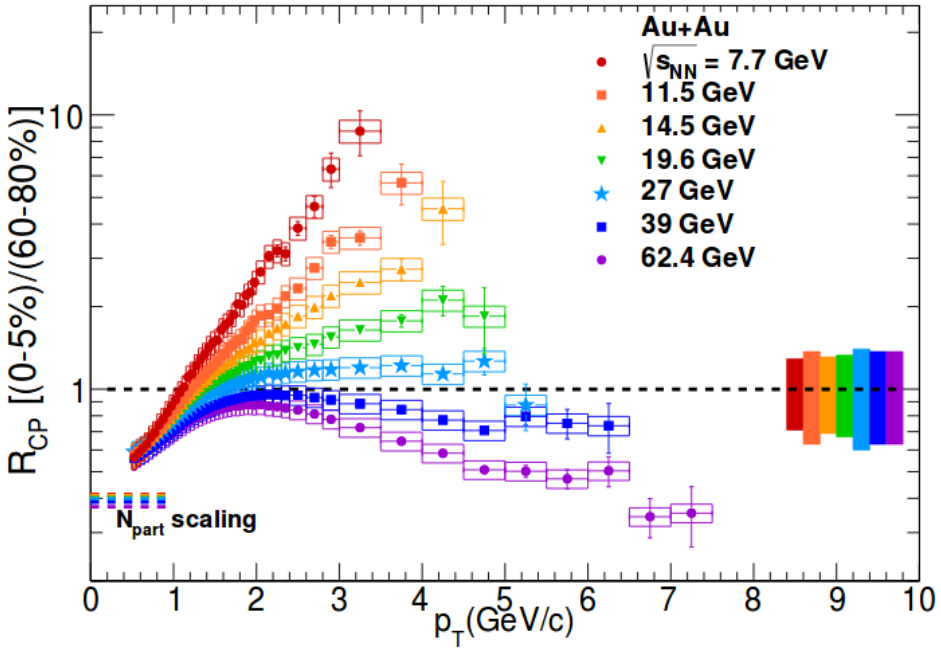

Di-hadron Correlations in Au+Au @ 200 GeV

Au+Au $\sqrt{s_{NN}}$ = 200 GeV
0-10%
- q_2 top 20%
- q_2 bottom 20%

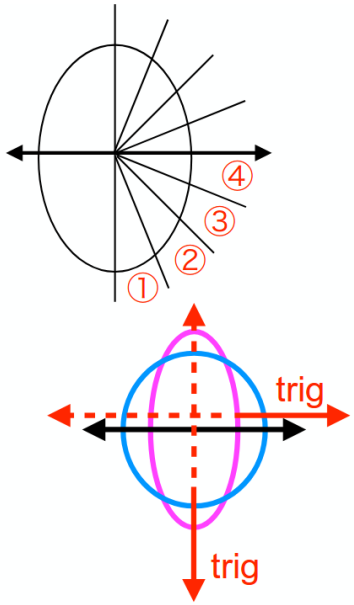

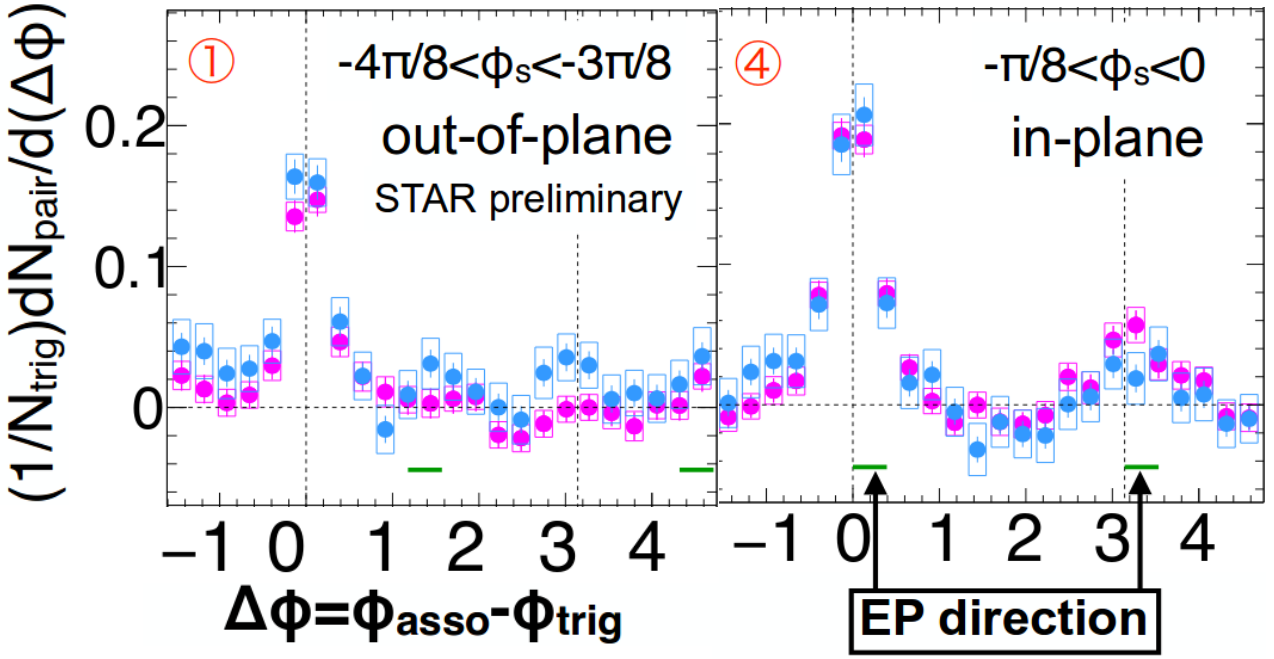

- High-p_T particles penetrate more with short pathlength
- Low-p_T particles are pushed toward in-plane direction and this effect is stronger in large q_2
  - Pathlength-dependent jet-medium interaction

“Hard Core” Di-Jets

$$A_J = \frac{p_T^{\mathrm{Lead}} - p_T^{\mathrm{SubLead}}}{p_T^{\mathrm{Lead}} + p_T^{\mathrm{SubLead}}}$$

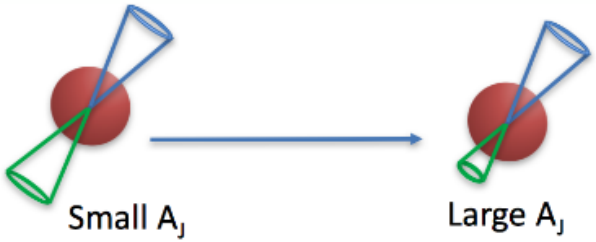

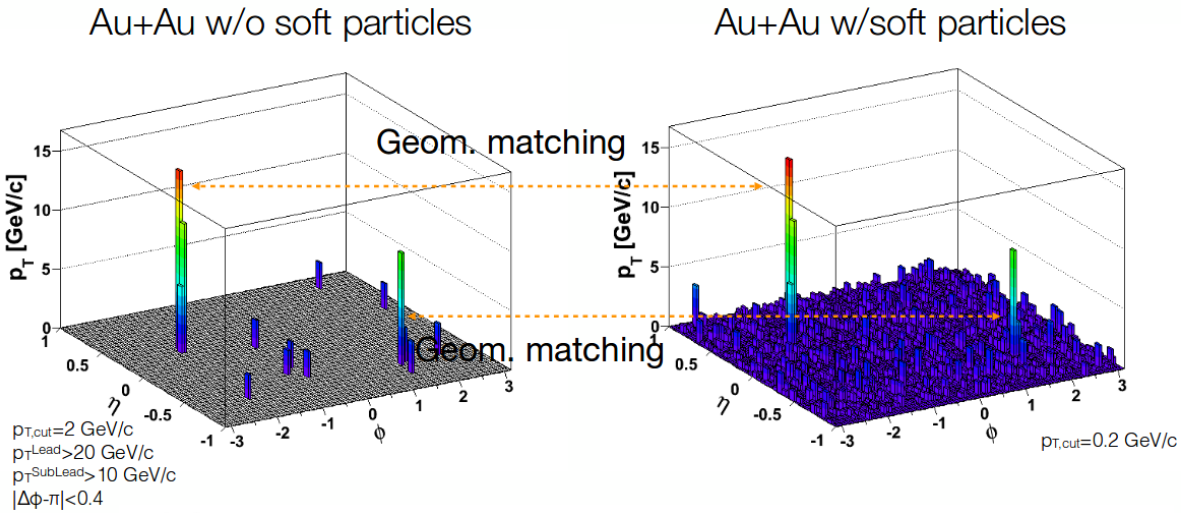

Momentum balance restored to p+p baseline for R=0.4, after adding particles with p<2 GeV/c

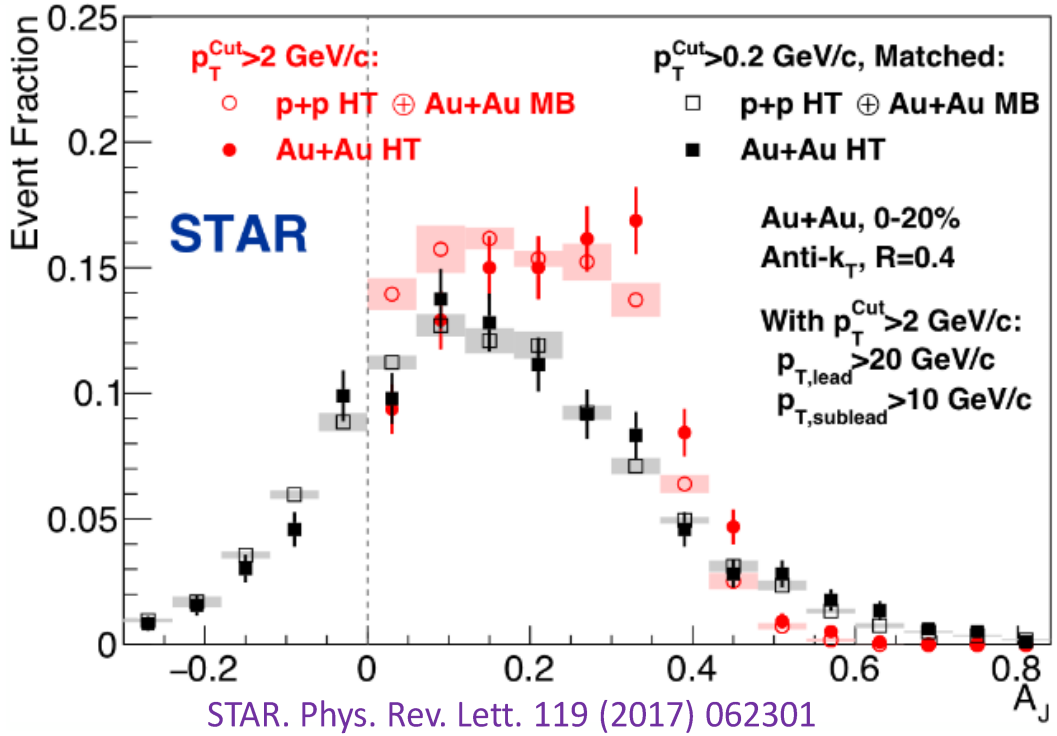

STAR. Phys. Rev. Lett. 119 (2017) 062301

The STAR Fixed-Target Program

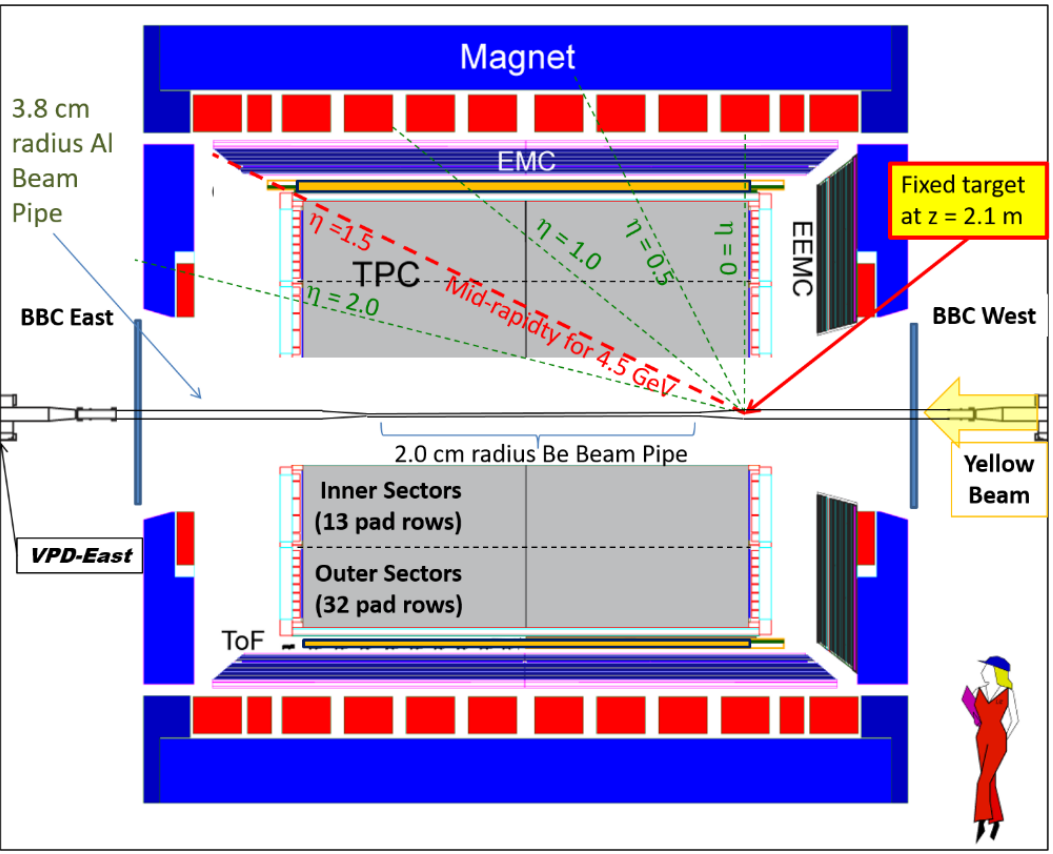

A 1 mm thick (4% inter. prob.) gold target

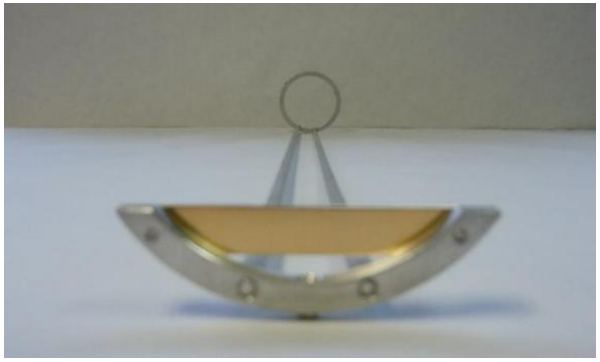

V_y vs. V_x Distribution

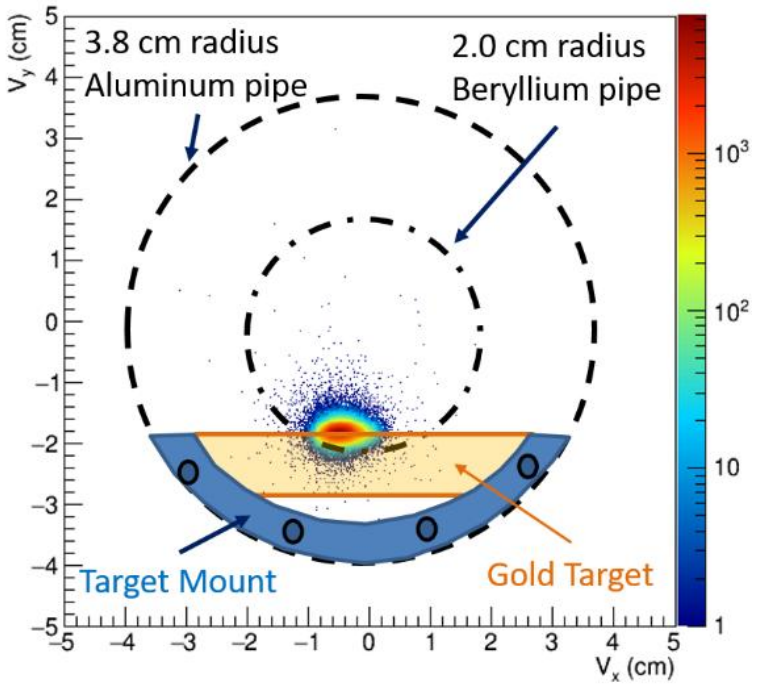

1.3M events from half hour test run, top 30% central trigger, Au+Au $\sqrt{s_{NN}}$=4.5 GeV

3.4M events from two hour test run, top 30% central trigger, Al+Au $\sqrt{s_{NN}}$= 4.9 GeV

Pion Spectra and dN/dy in Au+Au at $\sqrt{s_{NN}}$=4.5 GeV

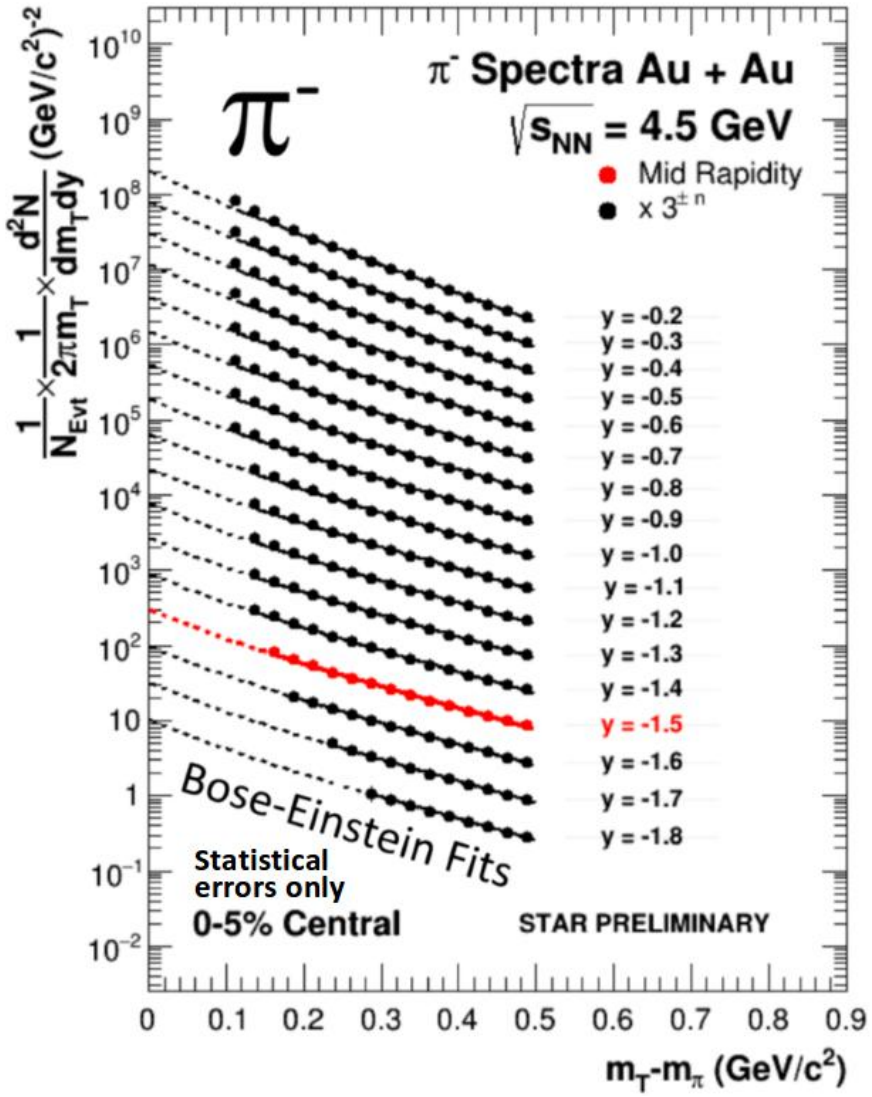

- Amplitudes & widths of rapidity densities are consistent with AGS experiments
- m_T–m_0 and y range will be extended by eTOF & iTPC upgrade

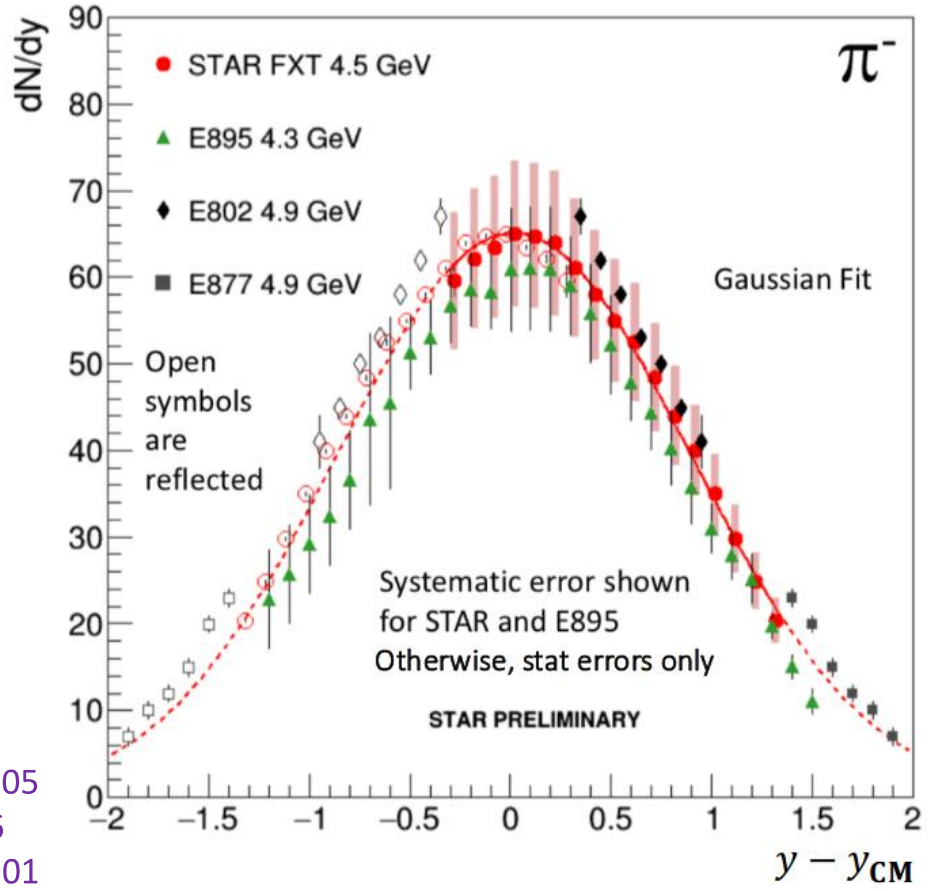

E895. Phys. Rev. C 68 (2003) 054905
E802. Phys. Rev. C 57 (1998) R466
E877. Phys. Rev. C 62 (2000) 024901

Directed Flow Measurements from FXT

E895. Phys. Rev. Lett. 84 (2000) 005488
STAR . Phys. Rev. Lett. 112 (2014) 162301

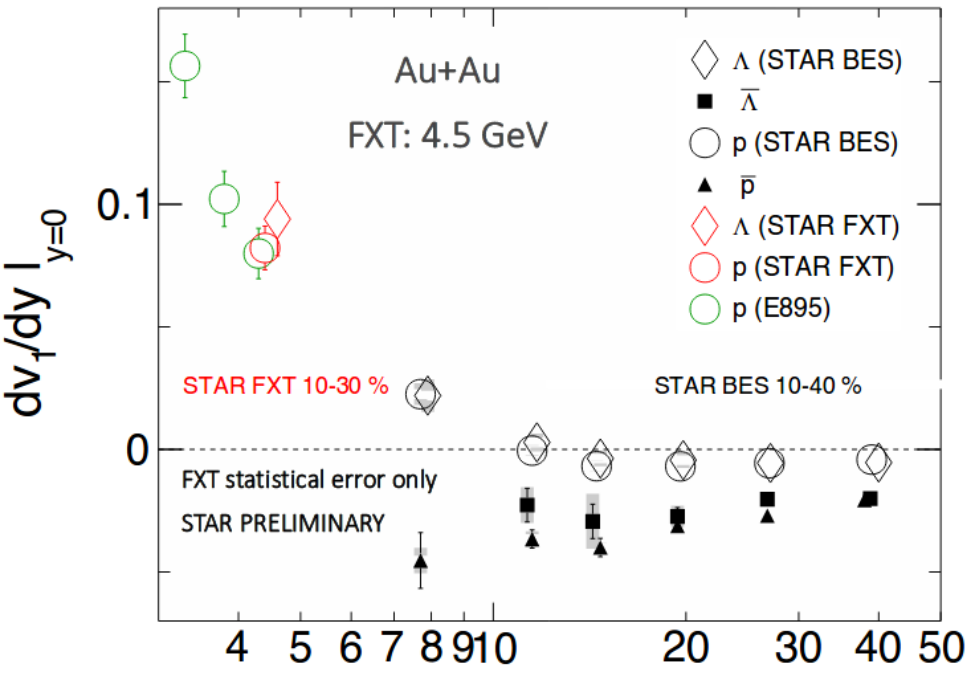

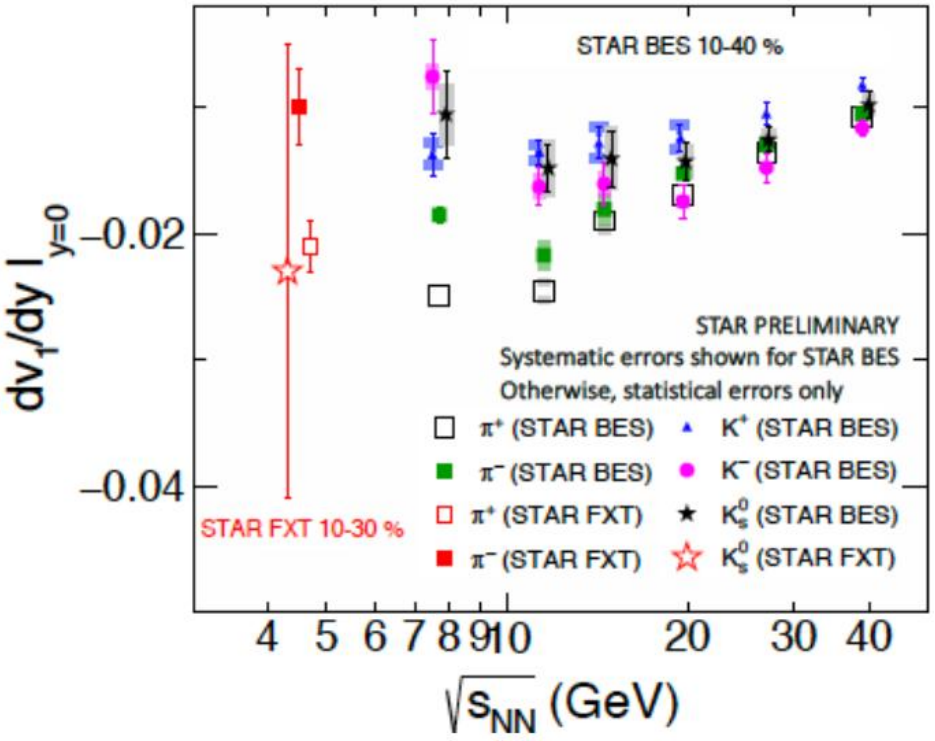

- Proton v_1 is consistent with E895. Λ v_1 is close to that of proton
- First pion v_1 measurements in this energy range
- π^+ π^- ordering supports the idea that transported quarks have bigger effect on π^-

Femtoscopic Measurements in FXT

E866. Phys. Rev. C 66 (2002) 054096
E895 .Phys. Rev. Lett. 84 (2000) 2798
ALICE. Phys. Rev. B 696 (2011) 328
STAR. Phys. Rev. C 92 (2015) 014904

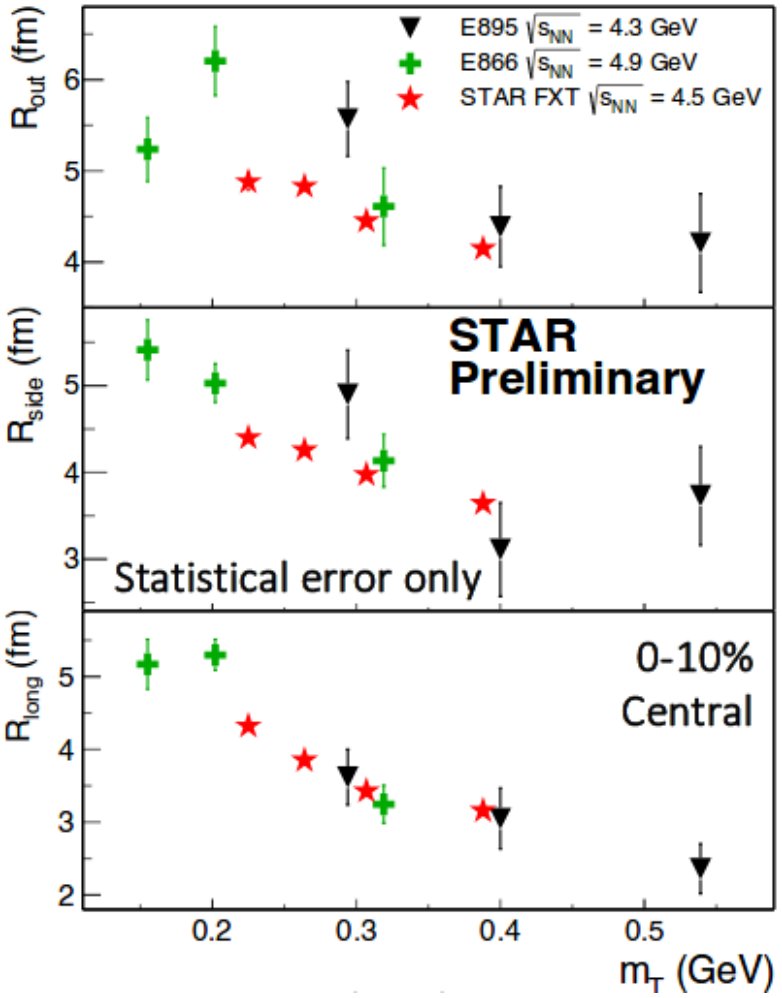

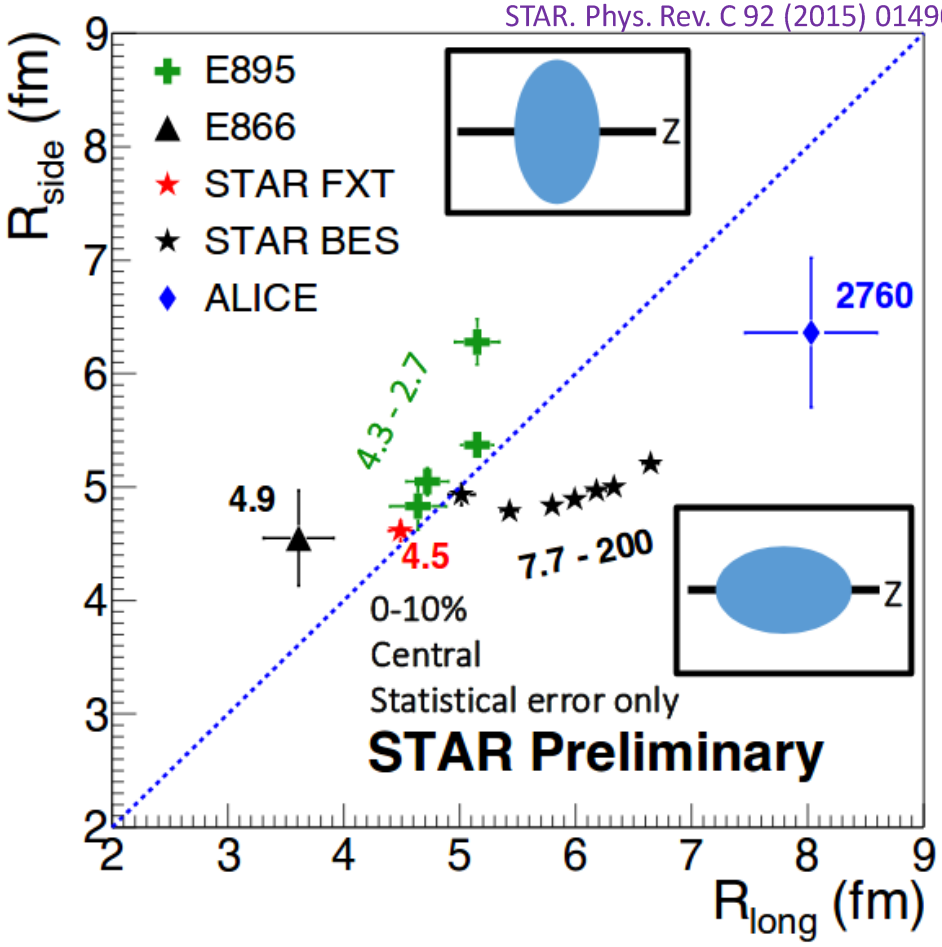

- Consistent with results from AGS experiments, with smaller stat. errors
- Apparent source shape evolves from oblate to prolate, as energy increases
- Increased longitudinal expansion above FXT energy

Upgrades for BES-II

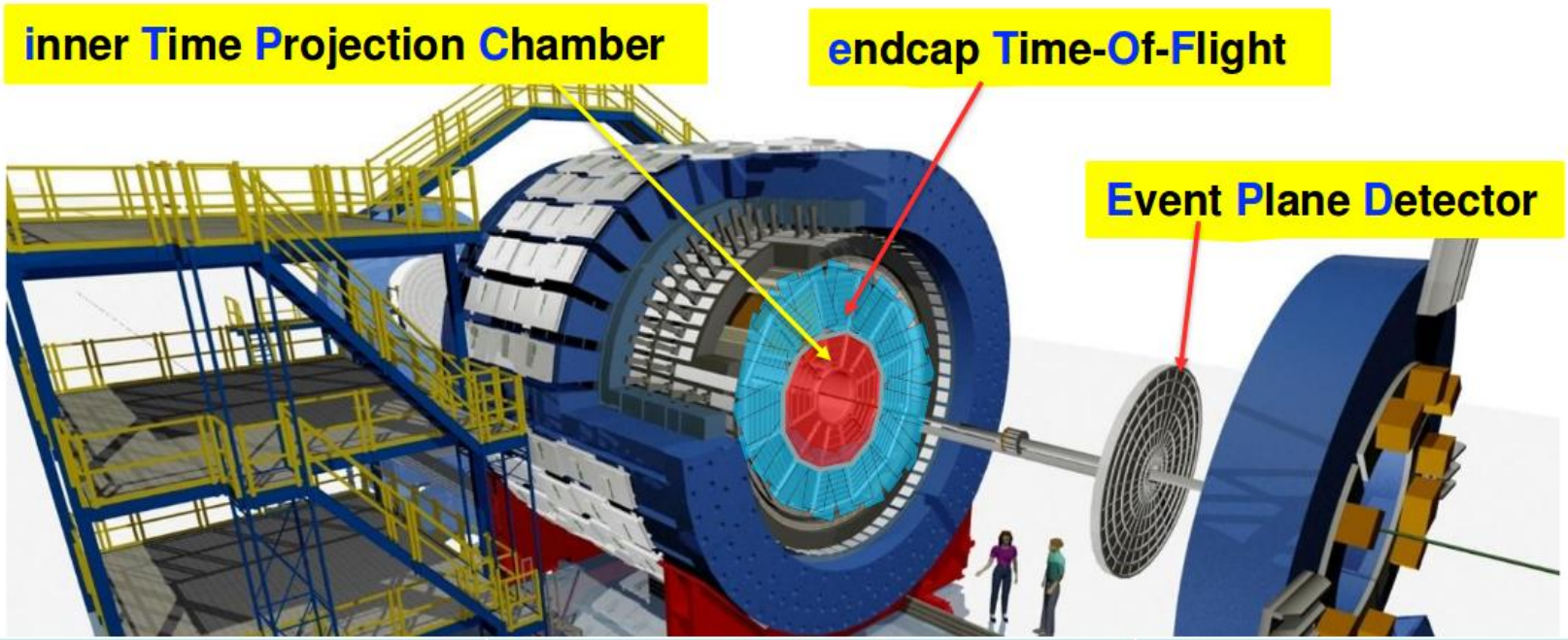

iTPC upgrade	eTOF upgrade	EPD upgrade
Continuous pad rows Replace all inner TPC sectors	**Add CBM TOF modules and electronics (FAIR Phase 0)**	**Replace Beam-Beam Counter**
$\|\eta\| < 1.5$	**$-1.6 < \eta < -1.1$**	**$2.1 < \|\eta\| < 5.1$**
$p_T > 60$ MeV/c	Extend forward PID capability	Better trigger & b/g reduction
Better dE/dx resolution Better momentum resolution	Allows higher energy range of Fixed-Target program	Greatly improved Event Plane info (esp. 1st-order EP)

Upgrades for BES-II

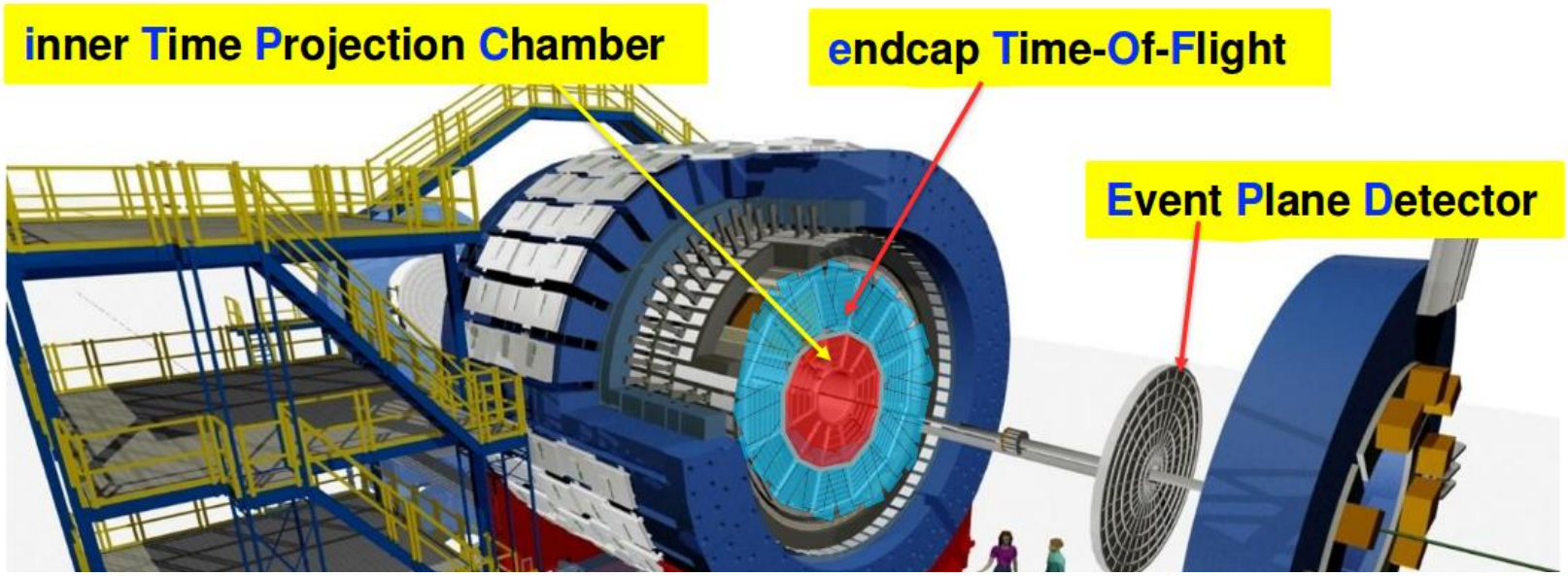


One iTPC sector has been installed


3 eTOF modules have been installed


Full EPD has been installed

The inner TPC upgrade

- **Inner Sectors**
  - New designed strongback
  - New wire frames
  - Increase readout pad rows (13 to 40)
- **New electronics for inner sectors**
  - Doubled readout channels. Using ALICE SAMPA chip
- **New designed insertion tooling**
  - Removal and insertion of inner sectors
- **Replace all 24 inner sectors**
  - 2018: One sector has been installed and used in the physics run
  - Full installation in autumn 2018

iTPC (one sector) performance in the current isobar collisions

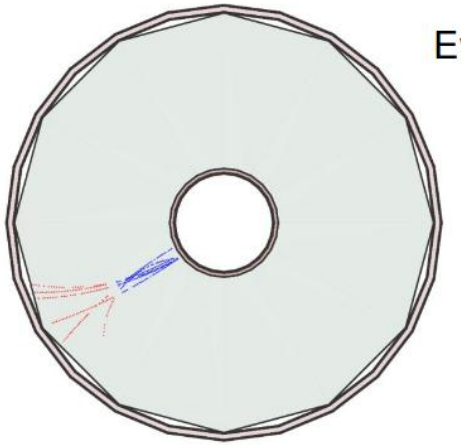

- Maximum hits per track: 45⟶72
- Lower transverse momentum threshold of 60 MeV/c
- η coverage extended by 0.4 units

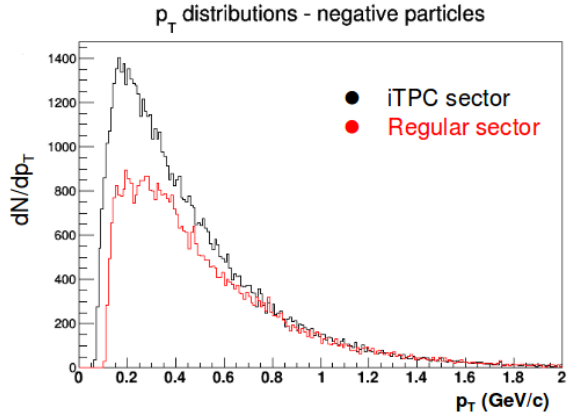

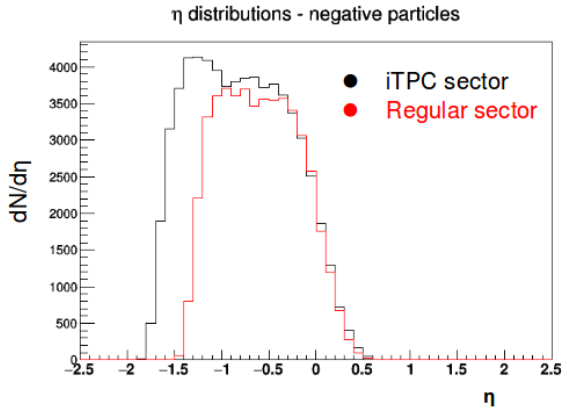

The endcap Time-Of-Flight

- **Install, commission and use 10% of the CBM TOF modules in STAR**
- **Design concept**
  - 3 layers, 12 sectors, 36 modules, 108 MRPCs
- **Provides PID in the forward direction**
  - Extended rapidity and yields
- **One sector with three modules has been installed for runs in 2018**
- **Full installation in autumn 2018**

eTOF (three modules) commissioned, integrated and participated in data taking

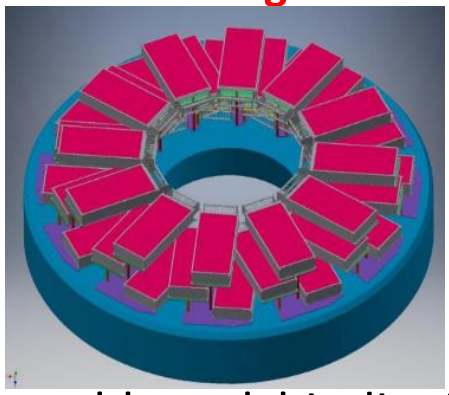

- Reasonable η-ϕ hit distribution
  - eTOF works properly
- Time resolution 59 ps

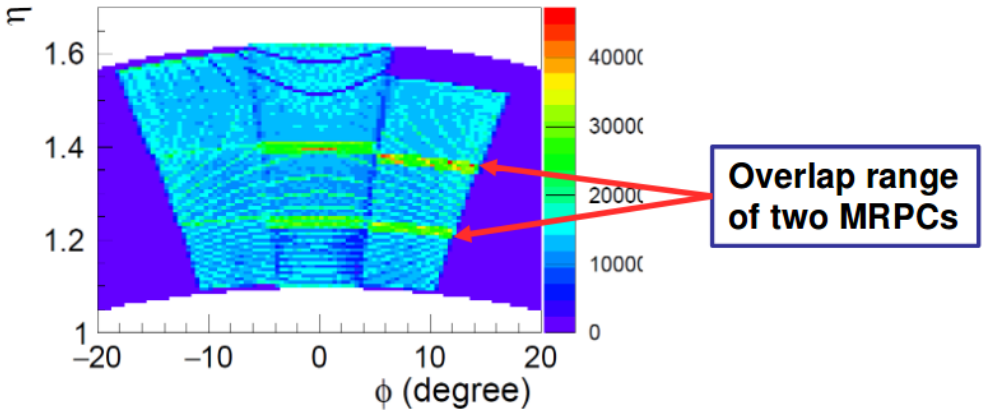

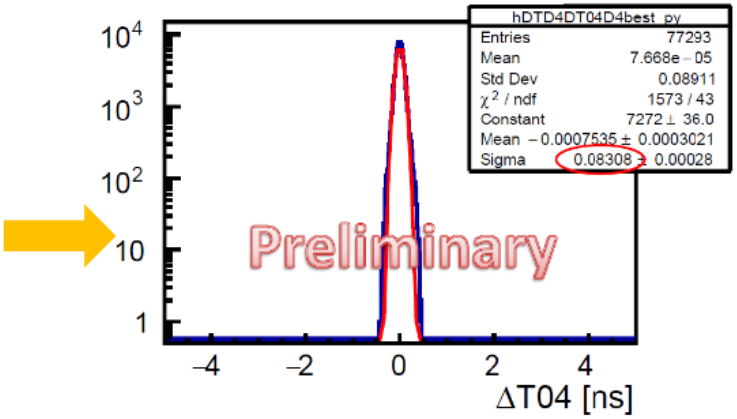

✓ System time resolution: 83 ps
✓ Counter time resolution: 59 ps

The Event Plane Detector

Event Plane Detector

- **2 wheels**
  - East and West EPD (2.1<|η|<5.1)
- **12 super sectors**
  - Scintillator wedges, milled to form 31 tiles
  - Optically separated by epoxy
- **Fiber optics**
  - Wavelength-shifting fibers
  - Grouped in 3D-printed connectors
- **Sensors**
  - Silicon Photon Multipliers (SiPM)

EPD is fully installed and took part in data taking in 2018

- All 744 tiles are good
- Good correlation between BBC and EPD
  - Correct timing
- Timing resolution is about 0.75 ns with fastest TAC method
  - 0.35 ns with average TAC method, raw slewing correction
- The 2nd-order event plane resolution is 0.37 in 20-30% central events at top energy isobar collisions

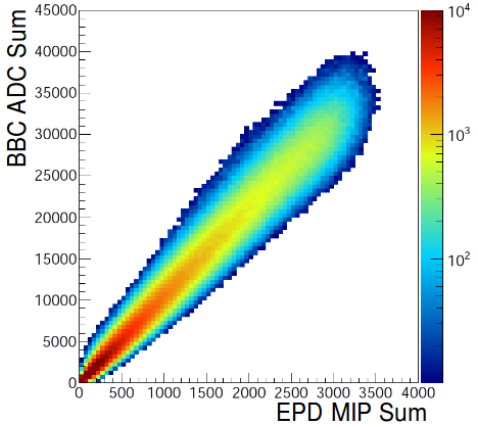

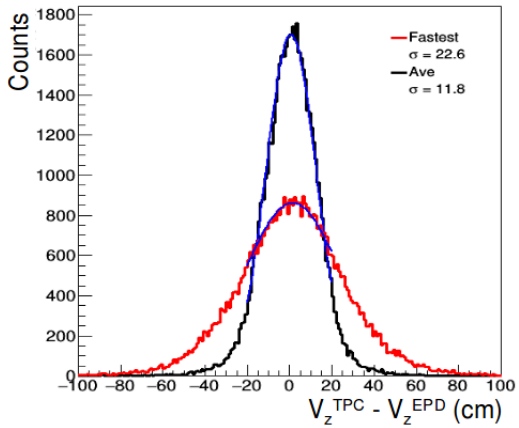

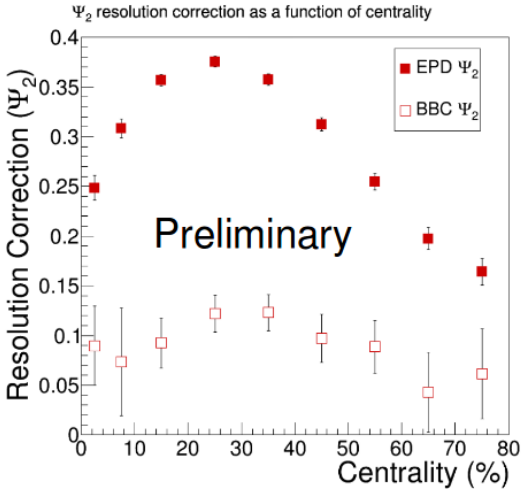

Short Term Plan

Year 2018:

- Took ~1.5B events for Zr+Zr and Ru+Ru collision systems each
- Au+Au data at 27 GeV (~500M events) and 3.0 GeV (~300M events)

✓ Physics goals: Chiral Magnetic Effect, global polarization, dileptons, etc..

Plan for 2019-2021:

Beam Energy (GeV/nucleon)	$\sqrt{s_{NN}}$ (GeV)	μ_B (MeV)	Run Time	Number Events
9.8	19.6	205	4.5 weeks	400M
7.3	14.5	260	5.5 weeks	300M
5.75	11.5	315	5 weeks	230M
4.55	9.1	370	9.5 weeks	160M
3.85	7.7	420	12 weeks	100M
31.2	7.7 (FXT)	420	2 days	100M
19.5	6.2 (FXT)	487	2 days	100M
13.5	5.2 (FXT)	541	2 days	100M
9.8	4.5 (FXT)	589	2 days	100M
7.3	3.9 (FXT)	633	2 days	100M
5.75	3.5 (FXT)	666	2 days	100M
4.55	3.2 (FXT)	699	2 days	100M
✓ 3.85	3.0 (FXT)	721	2 days	100M

The STAR Forward Upgrade (2021+)

Forward Calorimeter System:

- ECal: reuse PHENIX PbSC calorimeter with new readout on front phase
- HCal: sandwitch iron-scintillator plate sampling Calo

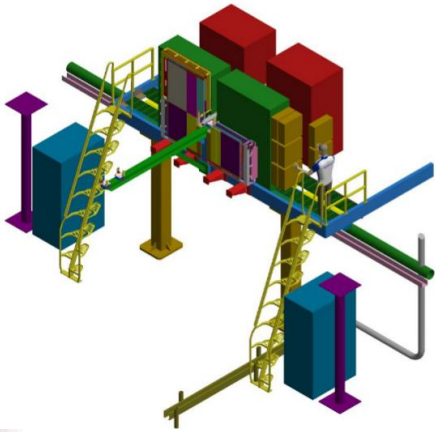

Forward Tracking System:

- 3 silicon disks: at 90, 140 and 187 cm from IR. Built on successful experience with STAR IST
  - Single-sided double-metal mini-strip sensors
  - Existing IST FEE, DAQ and cooling system
- 4 small-strip Thin Gas Chambers (sTGC): at 270, 300, 330, 360 cm from IP
  - Position resolution: $\sim$100 μm
  - Readout: reuse current STAR TPC electronics
  - The 1st sTGC prototype to be installed in STAR in 2019 (1/4 size of ATLAS sTGC)

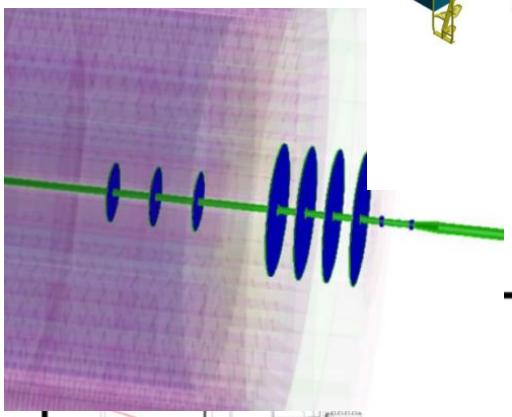

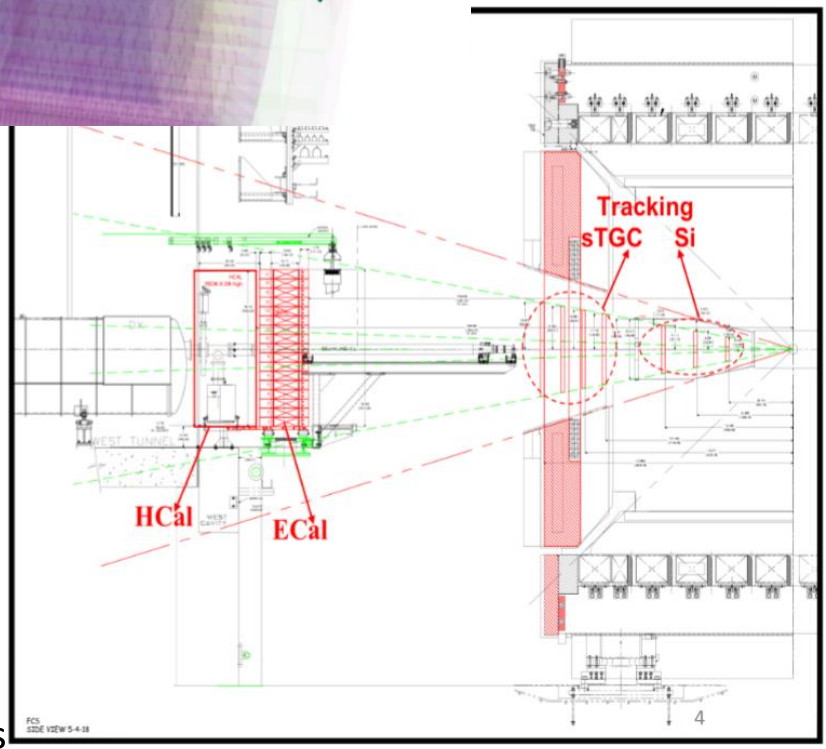

Physics:

- 3-dim. characterization of proton in momentum and spatial coordinates
- Di-jet measurements in the forward region (2.8< η <3.7)
- Gluon polarization at very low x (≤5×10^{-3})
- Nature of initial state and hadronization in nuclear collisions

Summary

- Collective dynamics and correlations
  - v_1, longitudinal flow decorrelation, femtoscopy
- Global and local hyperon polarization
- Particle production
  - Ultra-peripheral collisions, (anti)hypertriton, Λ_C, Upsilon R_{AA}
  - High-pT particles and jet modification
  - R_{CP} from BES-I, di-jet imbalance
- The STAR fixed-target results
- Detector upgrades

Backup slides

Directed flow measurements

10-40% Au+Au collisions

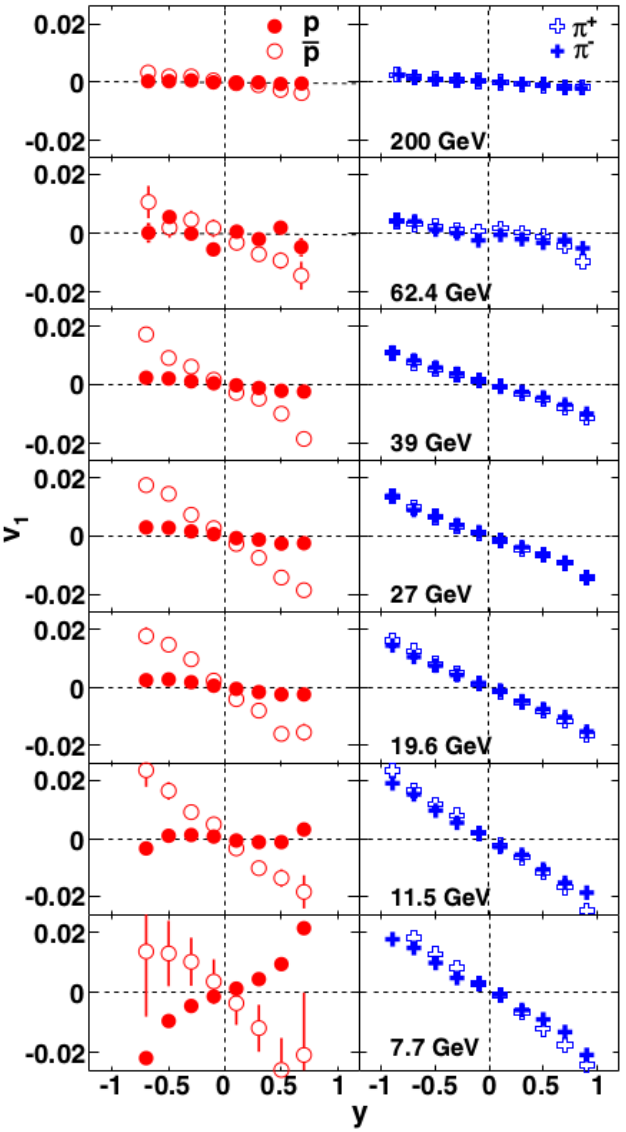

To extract v_1 slope, linear fit was used over $|y|<0.6$ for ϕ meson and over $|y|<0.8$ for all other species

STAR. Phys. Rev. Lett. 112 (2014) 162301
STAR. Phys. Rev. Lett. 120 (2018) 062301

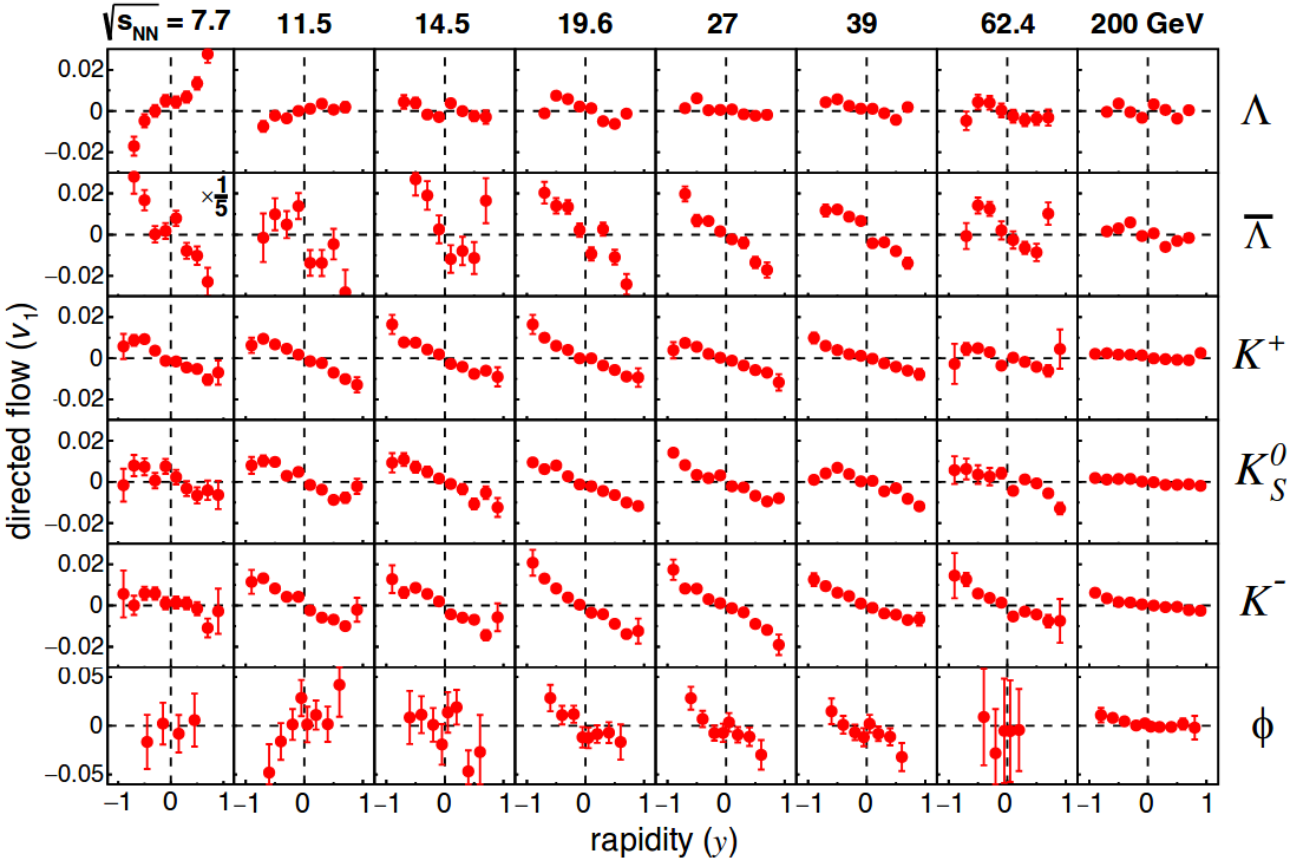

Global Hyperon Polarization

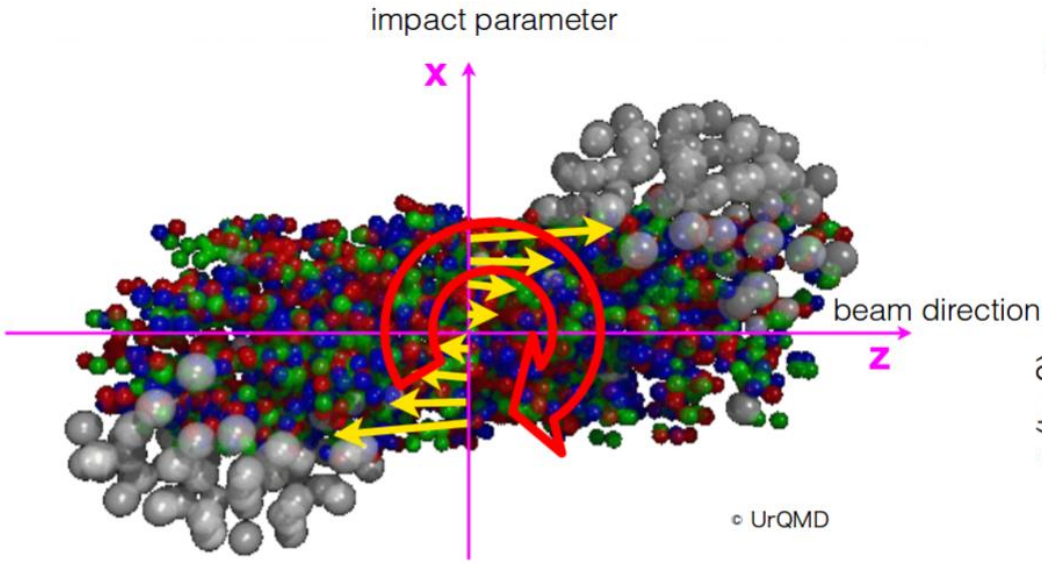

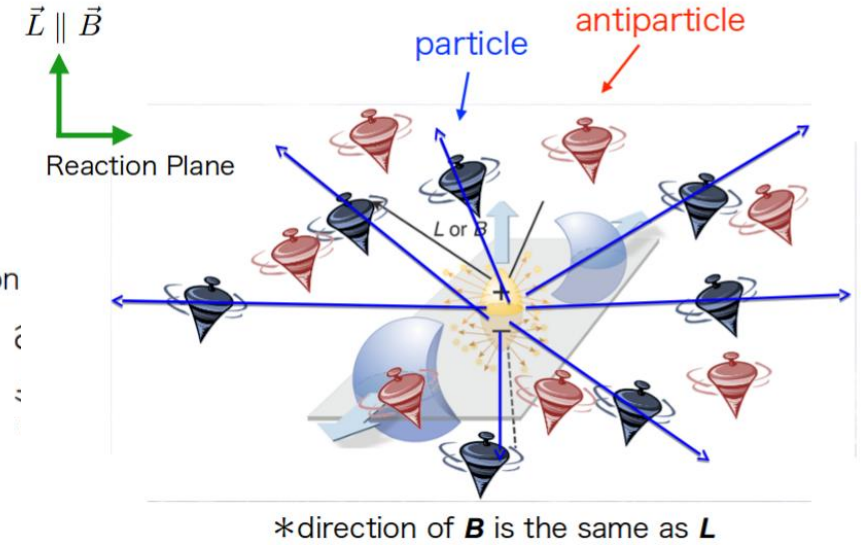

In non-central collisions, the initial collective longitudinal flow velocity depends on x:

$$\omega_y = \frac{1}{2}(\nabla \times v)_y \approx -\frac{1}{2}\frac{\partial v_z}{\partial x}$$

Non-zero angular momentum transfers to the spin degrees of freedom:

- Z.-T. Liang and X.-N. Wang, PRL94, 102301 (2005)
- S. Voloshin, nucl-th/0410089 (2004)

Polarization due to spin-orbit coupling :

- Particle' and anti-particle's spins are aligned with angular momentum **L**

Spin alignment by B-field:

- Particle and antiparticle's spins are aligned oppositely along **B** due to the opposite sign of magnetic moment